

NASA Contractor Report 3129

NASA  
CR  
3129  
c.1

# Frost Formation on an Airfoil: A Mathematical Model I

Mark Dietenberger, Prem Kumar, and James Luers

CONTRACT NAS8-31294  
APRIL 1979

**NASA**

TECH LIBRARY KAFB, NM  
0061927



# NASA Contractor Report 3129

## Frost Formation on an Airfoil: A Mathematical Model I

Mark Dietenberger, Prem Kumar, and James Luers  
*University of Dayton Research Institute*  
*Dayton, Ohio*

Prepared for  
Marshall Space Flight Center  
under Contract NAS8-31294



National Aeronautics  
and Space Administration

**Scientific and Technical  
Information Office**

1979



## TABLE OF CONTENTS

SECTION	PAGE
1 INTRODUCTION	1-1
2 DERIVATION OF THE FROST THERMAL CONDUCTIVITY	2-1
2.1 THE HEAT TRANSFER PROCESSES WITHIN THE FROST LAYER	2-1
2.1.1 Air - Ice Thermal Conductivity, $k_e$	2-4
2.1.2 Radiation Effective Conductivity, $k_r$	2-6
2.1.3 Water Vapor Effective Conductivity, $k_v$	2-7
2.1.4 Forced-Air Enthalpy Rate Term, $G_a C_p \frac{\partial T}{\partial x}$	2-13
2.2 APPROACHES FOR CALCULATING K	2-15
2.2.1 Brian, et al. Approach	2-15
2.2.2 White's Approach	2-16
2.2.3 Biguria and Wenzel's Approach	2-17
2.2.4 Jones and Parker's Approach	2-18
2.2.5 Summary of the Four Approaches	2-19
2.2.6 The UDRI Approach	2-23
3 HEAT AND MASS TRANSFER COEFFICIENTS	3-1
3.1 LAMINAR NATURAL CONVECTION	3-4
3.2 TURBULENT FORCED CONVECTION	3-5
3.3 SUMMARY OF HEAT AND MASS TRANSFER COEFFICIENT EQUATIONS	3-9
4 THE SIMULATION OF FROST FORMATION	4-1
4.1 FROST FORMATION MODEL	4-1
4.2 THE NUMERICAL SCHEME FOR THE FROST FORMATION MODEL	4-3
5 COMPARISON OF THE MODEL WITH THE AVAILABLE EXPERIMENTAL DATA	5-1
6 SUMMARY AND RECOMMENDATIONS	6-1
7 REFERENCES	7-1

## LIST OF FIGURES

FIGURE NO.		PAGE
1	Schematic Diagram of the Heat Transfer Processes in the Frost Layer	1-3
2	Water Mass Flux Versus Distance in Frost Layer (Brian, et al. data, Reference 1)	2-9
3	Water Mass Flux Versus Distance in Frost Layer (Yamakawa, et al. data, Reference 13)	2-10
4	Thermal Conductivity Versus Temperature at Ice Density	2-21
5	Thermal Conductivity Versus Temperature at Air Density	2-22
6	Thermal Conductivity Versus Frost Porosity at 211 °k	2-24
7	Frost Structure Model of the Present Work	2-25
8	Comparison of the Present Frost Thermal Conductivity Model with Experimental Data of Brian, et al. (Reference 1)	2-28
9	Relationship Between Nusselt's Number and Reynolds' Number (Reference 13)	3-7
10	Relationship Between Local Heat and Mass Transfer Coefficient (Reference 13)	3-8
11	Weight Versus Time for Brian et al. Data (Reference 1)	5-3
12	Density Versus Time for Brian et al. Data (Reference 1)	5-4
13	Thickness Versus Time for Brian et al. Data (Reference 1)	5-5
14	Weight Versus Time for Yamakawa, et al. Data (Reference 13)	5-8
15	Density Versus Time for Yamakawa, et al Data (Reference 13)	5-9
16	Thickness Versus Time for Yamakawa, et al. Data (Reference 13)	5-10

## LIST OF FIGURES (CONT.)

FIGURE NO.		PAGE
17	Weight Versus Time for Nakamura Data (Reference 14)	5-12
18	Density Versus Time for Nakamura Data (Reference 14)	5-13
19	Thickness Versus Time for Nakamura Data (Reference 14)	5-14

## LIST OF TABLES

TABLE NO.		PAGE
I	Summary of Approaches to Calculating Frost Thermal Conductivity	2-20
II	Data Input to the Frost Formation Model for Comparison With Brian et al. Data for Forced Convection (Reference 1)	5-2
III	Data Input to the Frost Formation Model for Comparison With Yamakawa, et al. Data for Forced Convection in a Duct (Reference 13)	5-7
IV	Data Input to the Frost Formation Model for Comparison With Nakamura Data for Natural Convection on Vertical Plate (Reference 14)	5-11

## List of Symbols

b	Linear dimension of ice crystals (cm)
$C_p$	Specific heat of air (J/g°C)
$C_{pf}$	Specific heat of frost (J/g°C)
D	Diffusion coefficient (cm <sup>2</sup> /s)
$\frac{D}{Dt}$	Total derivative = $\frac{\partial}{\partial t} + U_a \frac{\partial}{\partial x}$
$D_e$	Hydraulic diameter (cm)
$D_{eff}$	Effective diffusion coefficient of water vapor in the frost (mm <sup>2</sup> /s)
F	Blowing parameter
g	Gravitational acceleration (m/s <sup>2</sup> )
$G_a$	Air mass flow rate per unit area (g/m <sup>2</sup> s)
Gr	Grashof number
H	Height of plate (m)
$h_H$	Heat transfer coefficient (w/m <sup>2</sup> °C)
$h_m$	Mass transfer coefficient (g/m <sup>2</sup> s)
$h_H^*$	Experimental heat transfer coefficient (w/m <sup>2</sup> °C)
$h_m^*$	Experimental mass transfer coefficient (g/m <sup>2</sup> s)
i	Enthalpy (per unit mass)
K	Thermal conductivity of the frost (w/m°C)
k	Thermal conductivity of ice/air structure in the layer (w/m°C)
$k_a$	Thermal conductivity of air (w/m°C)
$k_b$	Thermal conductivity of air bubbles (w/m°C)
$k_c$	Thermal conductivity of ice cylinders (w/m°C)
$k_e$	Effective thermal conductivity of air-ice structure (w/m°C)
$k_{eff \text{ air}}$	Effective air thermal conductivity (w/m°C)

$k_i$	Thermal conductivity of ice (w/m°C)
$k_l$	Lower limit of thermal conductivity for air bubbles and ice cylinders (w/m°C)
$k_p$	Thermal conductivity of ice planes (w/m°C)
$k_r$	Radiation thermal conductivity (w/m°C)
$k_s$	Thermal conductivity of ice spheres (w/m°C)
$k_u$	Upper limit of thermal conductivity for air bubbles and ice cylinders (w/m°C)
$k_v$	Water vapor effective conductivity (w/m°C)
L	Latent heat, $L_e$ or $L_s$
$Le$	Lewis number
$L_e$	Latent heat of water evaporation (J/g)
$L_s$	Latent heat of ice sublimation (J/g)
$\dot{m}_d$	Water vapor mass flux within the frost layer ( $g/m^2s$ )
$\dot{m}_{d_s}$	Water vapor flux at the frost surface ( $g/m^2s$ )
$\dot{m}_{exp}$	Experimental value of water mass flux through the frost surface ( $g/m^2s$ )
$\dot{m}_t$	Total water mass flux in the frost layer ( $g/m^2s$ )
Nu	Nusselt number for forced convection
$Nu_H$	Nusselt number for natural convection based on plate height
$Nu_z$	Local Nusselt number for natural convection
P	Pressure ( $N/m^2$ )
Pr	Prandtl number
$P_t$	Total pressure ( $N/m^2$ )
$P_v$	Water vapor pressure ( $N/m^2$ )
$P_v^*$	Referenced pressure ( $N/m^2$ )
Q	Internal heat generated within the frost layer ( $w/m^3$ )

$q_o$	Constant heat flux at the wall ( $w/m^2$ )
$q_r$	Radiation heat flux vector ( $w/m^2$ )
Re	Reynolds number based on hydraulic diameter
$R_v$	Water vapor gas constant = $4.6150 \times 10^6$ erg/ $C^2g$
Sc	Schmidt number
$Sh_H$	The Sherwood number for natural convection based on height of plate
St	Stanton number
T	Temperature ( $^{\circ}K$ )
t	Time (s)
$T_a$	Ambient air temperature ( $^{\circ}K$ )
$T_s$	Frost surface temperature ( $^{\circ}K$ )
$T_w$	Wall temperature ( $^{\circ}K$ )
$T^*$	Referenced temperature ( $^{\circ}K$ )
$U_a$	Air velocity (m/s)
x	Distance from the wall (m)
$x_s$	Frost thickness (cm)
$\alpha$	$k_{eff\ air}/k_i$
$\beta$	Porosity of frost
$\beta_c$	Proportion of frost volume representing ice spheres and ice planes
$\epsilon$	Emissivity of frost
$\theta$	Fractional volume of ice fragments
$\theta_c$	Proportion of frost volume representing ice cylinders and air bubbles
$\rho_a$	Air density (g/cc)
$\rho_f$	Mass density of frost (g/cc)
$\rho_v$	Water vapor density (g/cc)

$\rho_{vs}$	Density of water vapor at frost surface (g/cc)
$\sigma$	Stefan-Boltzmann constant = $0.56697 \times 10^{-8} \text{ w/m}^2/\text{°C}^4$
$\tau_s$	Tortuosity
$\nu$	Kinematic viscosity
$\phi_a$	Relative humidity in ambient air
$\chi$	Relative concentration (moles $\text{H}_2\text{O}$ /moles air)
$\omega_a$	absolute ambient humidity
$\omega_s$	frost surface absolute humidity
$\omega_w$	absolute saturated humidity at wall temperature

## FOREWORD

The research in this document is intended to contribute toward a quantitative assessment of the aerodynamic penalties on an aircraft with frost coated wings during takeoff. The frost problem is serious for both general aviation and air carriers. For air carriers it is an economic hardship because of the expense involved in removing frost prior to takeoff. For general aviation it is a potential safety hazard since takeoffs are permitted with frost. The objective of the UDRI research effort, of which this report constitutes the first task, is to quantify the safety hazards of frost so that realistic takeoff procedures and guidelines can be established. In the future, the model will be used for a twelve hour advance prediction of the density and thickness of morning accumulation of frost on an airfoil. The model will also be used as part of an aircraft simulation program under a frosted wing condition to determine the dissipation of frost during takeoff and climbout.

This research was conducted by the UDRI for NASA/George C. Marshall Space Flight Center, Huntsville, Alabama, under the technical direction of Mr. Dennis Camp of the Space Science Laboratory. The support for this research was provided by Mr. John Enders of the Aeronautical Operating Systems Division, Office of Advanced Research and Technology, NASA/Headquarters.

SECTION 1  
INTRODUCTION

In colder climates the overnight frost accumulation on an aircraft is a common occurrence. To ensure safe takeoff, Federal Air Regulations require that frost be removed from commercial aircraft. Frost removal is a costly and time consuming process that perhaps could be avoided if better information were available about the frost formation, its dissipation, and its aerodynamic effects on takeoff. For general aviation, takeoffs are permitted with a frosted wing surface. Safety records indicate, however, that many takeoff accidents are attributable to the aerodynamic penalties associated with a frost roughened airfoil.

Very little quantitative data exists concerning the aerodynamic penalties associated with frost on an aircraft wing. In many cases a completely safe takeoff may be possible if the frost layer is sufficiently thin. In other cases where aerodynamic penalties are significant, a safe takeoff may still be possible at a reduced takeoff weight or with a sufficiently long runway. An additional area of concern for the aviation industry is the frost forecast. An accurate forecast of the frost severity on the eve of the frost would allow for adequate personnel, equipment, and supplies to be on hand for the frost removal exercise in the morning, or for some frost prevention procedure to be applied.

The aerodynamic penalties resulting from frost accumulation have not been studied in detail due, apparently, to the three-dimensional nature of the flow problem. Also, the complexity of the frost formation process appears to be one of the reasons that a satisfactory numerical frost model is not in existence. Frost formation has been investigated experimentally for numerous flows over flat surfaces and deposition configurations by several investigators. However, little correlation exists between theory

and experiments and this is probably the reason that no general theory can be found.

In this work, analysis of frost formation and its effect on takeoff aerodynamics proceeds by considering a more simple problem and then generalizing to more complex situations. The wing is first approximated as a flat plate and the flow around it is taken to be two-dimensional. The present study is made for three separate phases viz: 1) overnight formation and accumulation of frost on a flat plate; 2) modification of Phase I for the wing of the aircraft; and 3) the effect of accumulated frost on the wings during takeoff and the resulting aerodynamic penalties. Only the first phase is considered in this report. The study regarding the other two phases will be contained in future reports. The flat plate model developed in Phase I will be used for an airfoil in Phase II. It is anticipated that the two-dimensional approach can be extended to three dimensions once the complexities and the difficulties inherent in the present problem are analyzed.

Frost is formed when moist air comes into contact with cold surfaces having temperatures below both the dew point and the freezing point. The determination of the overnight accumulation of frost on a flat plate is a complex heat and mass transfer problem. Radiation cooling to space off the top side of the metallic surface causes it to cool faster than the surrounding air. When the metallic surface reaches a frost point temperature, frost formation begins. Additional cooling then increases the frost density and its thickness. The frost accumulation eventually forms an insulation between the metallic surface and space and thus an equilibrium condition may be reached wherein the frost surface temperature remains constant. The important heat transfer processes shown in Figure 1 are the radiative cooling to space, conduction from the wing surface through the frost to the air, the natural convection of heat to the frost surface, and the internal enthalpy rate within the frost. The change of state

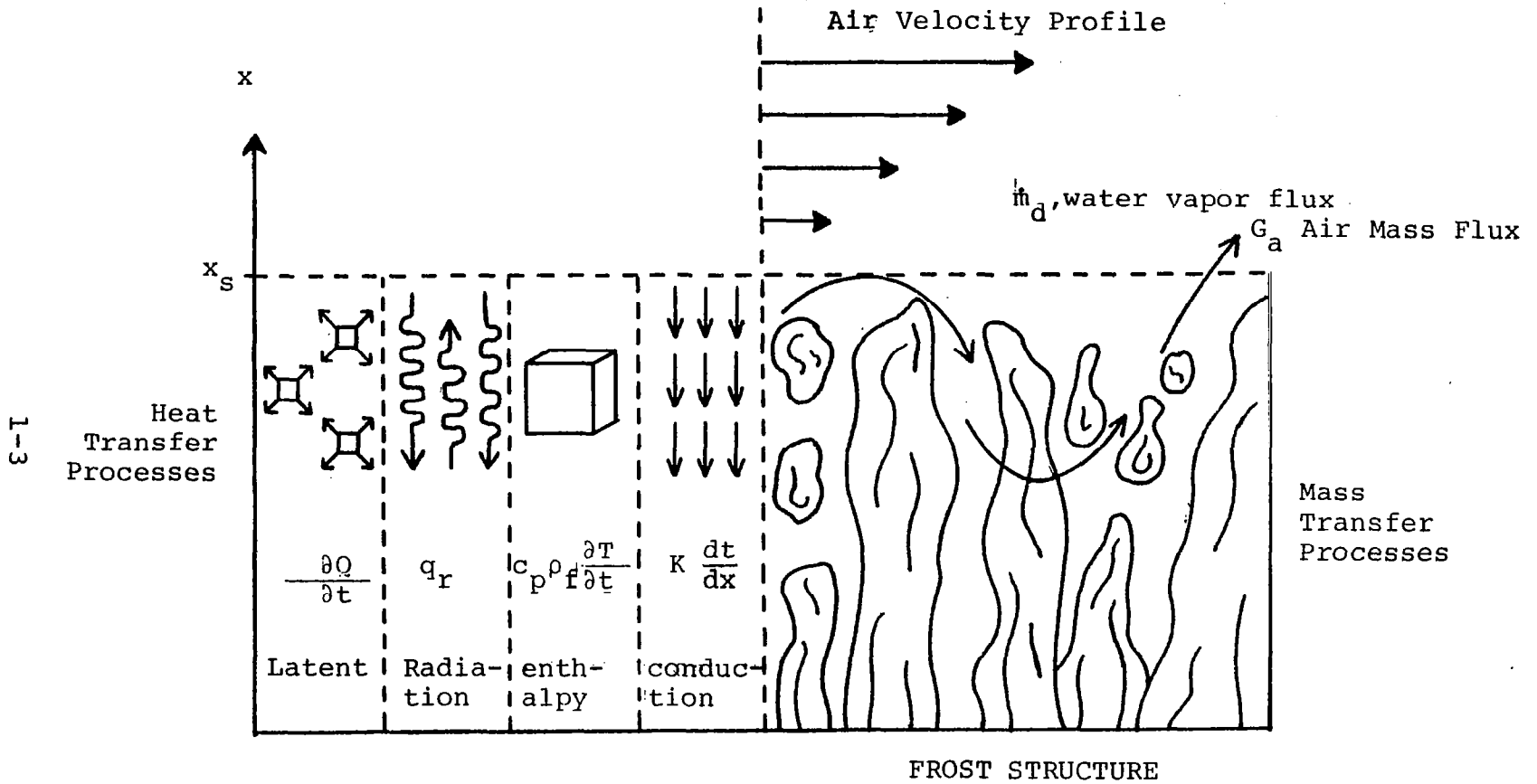


Figure 1. Schematic diagram of the heat transfer processes in the frost layer

from water vapor to frost introduces an important heat source within the frost layer, the latent heat of sublimation.

The nature of the frost formation process is sufficiently complicated so that it is difficult to predict the rate of formation and its density at a particular time. Many of the important characteristics of the frost depend on how it was formed. This history dependent nature of frost formation forbids the use of common types of correlations for predicting heat transfer rates used in other heat and mass transfer problems. Ordinarily, if the surface temperature is known, the heat transfer from the moist air to the surface can be calculated. Thus, if it is possible to describe adequately the heat transfer through the frost, then one can find the frost surface temperature by matching the heat transfer rate through the frost with the convective heat transfer. The description of the heat transfer rate through the frost requires a knowledge of the thermal conductivity and the history of formation of the frost which have not been adequately treated to date. Section 2 of this report is devoted to a treatment of the thermal conductivity and a new expression is presented. Section 3 analyzes the heat and mass transfer coefficients and gives modified relations which can be used more accurately for the transfer coefficients at the frost surface. In Section 4, a model is presented for predicting the growth rate of a frost layer using the analysis of the previous sections. Since the equations so developed cannot be solved analytically, numerical techniques have been applied to solve them. These techniques are also presented in Section 4. In Section 5 the results from the numerical model are compared with the experimental data available on frost formation. Considering the complexity of the problem, the results are very encouraging.

## SECTION 2

### DERIVATION OF THE FROST THERMAL CONDUCTIVITY

The thermal conductivity of the frost layer plays an important part in its structure and rate of formation. A number of authors addressed the problem of computing the frost thermal conductivity (References 1, 2, 3, 4, and 5). In this section, the various approaches used by these authors are examined by analyzing the underlying assumptions of each treatment. To fully understand these assumptions it is necessary to begin with a discussion of all possible heat transfer processes within the frost layer and to determine which processes are significant and which can be safely neglected. From this perspective, the different approaches taken by the authors can be evaluated and their results compared with experimental data. Furthermore, the range of environmental conditions will be determined for which a particular approach is realistic and the limitations of each approach can then be deduced. It will be shown that none of the present approaches are sufficient for a general frost model. As a result, a new, more comprehensive method of calculation the frost thermal conductivity based on the experimental data will be developed.

#### 2.1 THE HEAT TRANSFER PROCESSES WITHIN THE FROST LAYER

The various approaches to modeling of the frost temperature distribution and thus also the frost thermal conductivity can be derived from expressing the different heat transfer processes within the frost layer as shown in Figure 1. The expression for the energy equation for a control volume is given by (Reference 6)

$$\rho_f \frac{Di}{Dt} = \frac{DP}{Dt} + \frac{\partial Q}{\partial t} + \nabla \cdot (k \nabla T) + \nabla q_r \quad , \quad (1)$$

where  $\frac{D}{Dt}$  is the total derivative =  $\frac{\partial}{\partial t} + U_a \frac{\partial}{\partial x}$  ,

$\rho_f$  is the mass density of the frost layer (g/cc),

$t$  is time (s),

- $i$  is enthalpy (per unit mass),  
 $P$  is pressure ( $\text{N/m}^2$ ),  
 $Q$  is internal heat generation within the layer ( $\text{w/m}^3$ ),  
 $k$  is the thermal conductivity of ice/air structure in the layer ( $\text{w/m}^\circ\text{C}$ ),  
 $T$  is temperature ( $^\circ\text{K}$ ), and  
 $q_r$  is the radiation heat flux vector ( $\text{w/m}^2\text{s}$ ).

For heat transfer within a frost layer the following assumptions are made.

- 1 Within the frost layer, the temperature and the pressure are in a quasi-steady state, i.e., within a time interval  $\Delta t$

$$\rho_f c_{pf} \frac{\partial T}{\partial t} = \frac{DP}{Dt} = 0 \quad . \quad (2)$$

This assumption is based on experimental data by J. White (Reference 7). White has shown that the temperature and the pressure in the frost layer are at most slowly varying functions of time, partly due to the isothermal conditions of the wall and the upper limit of the frost surface temperature at melting point. Then, the energy storage rate is small compared with the heat flux; thus the justification of the assumption of quasi-steady state.

- 2 The internal heat generation rate produced by the phase change is given by

$$\frac{\partial Q}{\partial t} = L \frac{\partial \dot{m}_d}{\partial x} \quad , \quad (3)$$

where  $L = L_e$  or  $L_s$  and

$L_e$  is the latent heat of water evaporation ( $\text{J/g}$ ),

$L_s$  is the latent heat of ice sublimation ( $\text{J/g}$ ),

$\dot{m}_d$  is the water vapor mass flux within the frost layer ( $\text{g/m}^2\text{s}$ ), and

$x$  is the distance from the wall (m).

- 3 The enthalpy change produced by forced air flow through the frost structure is given by

$$G_a C_p \frac{\partial T}{\partial x} = \rho_d U_a \frac{\partial i}{\partial x} \quad , \quad (4)$$

where  $G_a$  is the air mass flow rate per unit area ( $\text{g}/\text{sm}^2$ )

$C_p$  is the specific heat of air ( $\text{J}/\text{g}^\circ\text{C}$ ), and

$U_a$  is the air velocity ( $\text{m}/\text{s}$ ).

- 4 The heat conduction is one-dimensional (through the layer to the wall) and the effective thermal conductivity,  $k_e$ , is a function of the combined heat conducting proportions of air and ice. This gives

$$(k\nabla T) = (k_e \frac{\partial T}{\partial x}). \quad (5)$$

- 5 The radiation heat flux is one-dimensional,

$$q_r = k_r \frac{\partial T}{\partial x} \quad (6)$$

where  $k_r$  = radiation thermal conductivity based on the Stefan-Boltzman law and the geometric view factors.

Under these assumptions the energy Equation (1) becomes

$$\frac{d}{dx} [(k_e + k_r) \frac{dT}{dx}] = -L \frac{d\dot{m}_d}{dx} - G_a C_p \frac{dT}{dx}. \quad (7)$$

A familiarity with the above energy equation by order of magnitude calculations is needed. More specifically, four terms,  $k_e$ ,  $k_r$ ,  $\dot{m}_d$ , and  $G_a$ , will be investigated in the above equation. It will be demonstrated that the heat flux represented by the radiation and the forced air enthalpy transport are negligible in comparison to the thermal conductivity of air-ice structure and the latent heat release of the waper vapor.

Since it will be shown that the thermal conductivity of air-ice structure contributes the largest of the four heat fluxes, the extreme values of  $k_e$  are used as a reference comparison for the order of magnitude calculations. The extreme values are the thermal conductivity of ice (Reference 8)

$$k_i = 630/T, \quad (8)$$

and the thermal conductivity of air (Reference 6)

$$k_a = 2.646 \times 10^{-3} \left( \frac{T^{1/2}}{1 + (\frac{245}{T}) 10^{-12/T}} \right). \quad (9)$$

### 2.1.1 Air - Ice Thermal Conductivity, $k_e$

As the frost contains air and the crystals of ice, the conductivity of frost should be somewhere between the thermal conductivities of air and ice. In the limit, depending on its density, it should approach the thermal conductivity of air or ice. Thus, the thermal conductivity of frost is defined in terms of the weighted functional relationship between the thermal conductivities of air and ice based on the density and the structure of the frost. Biguria and Wenzel (Reference 3) have compiled several theoretical models for different systems to formulate the effective thermal conductivity of the frost based on various assumptions for the frost structure. These expressions as applied to the air and ice phases are given as follows.

1. Resistance in series for minimum possible conductivity:

$$\frac{1}{k_{emin}} = \frac{1-\beta}{k_i} + \frac{\beta}{k_a} \quad , \quad (10)$$

where  $\beta$  is the porosity of frost.

2. Resistances in parallel for maximum possible conductivity:

$$k_{emax} = (1-\beta)k_i + \beta k_a \quad . \quad (11)$$

3. Russel equation for porous media where the solid (ice) is in a continuous structure and there is a distribution of cubical pores arranged in a simple cubic lattice:

$$\frac{k_e}{k_i} = \frac{\alpha\beta^{2/3} + 1 - \beta^{2/3}}{\alpha(\beta^{2/3} - \beta) + 1 - \beta^{2/3} + \beta} \quad , \quad (12)$$

with  $\alpha = k_a/k_i$  and  $\theta = 1-\beta$ .

4. Maxwell - Rayleigh equation for the case of fluid pores (air) distributed in a continuous solid (ice):

$$\frac{k_e}{k_i} = \left[ 1 - 2\beta \left( \frac{1-\alpha}{2+\alpha} \right) \right] / \left[ 1 + \beta \left( \frac{1-\alpha}{2+\alpha} \right) \right] \quad . \quad (13)$$

5. Maxwell-Rayleigh equation for the case of solid pores (ice) distributed in a continuous fluid (air):

$$\frac{k_e}{k_i} = \left[ 3 + 2\beta(\alpha - 1) \right] / \left[ 3 - \beta \left( \frac{\alpha - 1}{\alpha} \right) \right] \quad (14)$$

6. If one phase of the constituents (say ice or air) is not spatially continuous the Brailsford-Major equation gives:

$$k_e = \frac{1}{4} \left\{ (3\beta - 1)k_a + (3\theta - 1)k_i + \left[ \left( (3\beta - 1)k_a + (3\theta - 1)k_i \right)^2 + 8k_a k_i \right]^{1/2} \right\} \quad (15)$$

7. Woodside equation for a cubic lattice of uniform solid spherical particles (ice) in a gas (air):

$$\frac{k_a}{k_e} = 1 - \left( \frac{6\theta}{\pi} \right)^{1/3} \left[ 1 - \frac{a^2 - 1}{a} \log \left( \frac{a+1}{a-1} \right) \right] \quad (16)$$

$$\text{where } a = 1 + \left\{ \frac{4}{\pi \left( \frac{1}{\alpha} - 1 \right) \left( \frac{6\theta}{\alpha} \right)^{2/3}} \right\}^{1/2}$$

for  $0 \leq \theta \leq 0.5236$ .

In their observations of frost formation, Brain, et al. (Reference 1) found that the initial frost dendrites are spherical in shape at about 5 to 10 $\mu$  in diameter. As smooth frost forms, the diameters become about 20 to 50  $\mu$  and the ice dendrites begin to mesh together. Biguria and Wenzel (Reference 3) observed that initial frost was rough, consisting of ice trees and air spaces. They assumed that parallel heat transfer could be dominant up to a frost density of 0.02 g/cc. Then from 0.02 g/cc to 0.05 g/cc, the thermal conductivity was observed to decrease since parallel heat transfer was no longer valid when the frost formed a close-knit mesh of dendrites. Then at densities greater than 0.05 g/cc, the dendrites begin to enclose air pockets. Thus a realistic frost structure model should be spatially

continuous both in the air and the ice phases. Note that none of these seven theoretical thermal conductivity expressions directly provide for such a structure.

Given the complexity of deriving an expression of  $k_e$  for a realistic frost structure, one wonders if it is useless to list Equations (10) to (16) and attempt a theoretical approach toward the frost thermal conductivity. Later, an entirely empirical approach will be found to be of little value also. Finally, a semi-theoretical approach which makes indirect use of Equations (10), (11), (13), (14), and (15) will be derived to reflect a realistic frost structure. At this point it is important to understand that  $k_e$  is the air-ice thermal conductivity. The frost thermal conductivity is an expression that will be derived to take into account the other heat flux terms in Equation (7).

### 2.1.2 Radiation Effective Conductivity, $k_r$

The radiation effective conductivity can be shown to be negligible for the size of the ice crystals and the temperatures in the frost layer by the following argument. The radiation effective conductivity as given by Laubitz (Reference 9) is

$$k_r = 4\sigma T^3 \epsilon \frac{b}{\theta} (1 - \theta^{2/3} + \theta^{4/3}) \quad , \quad (17)$$

where  $\sigma$  is Stefan-Boltzmann constant =  $0.56697 \times 10^{-8} \text{ w/m}^2/\text{°C}^4$ ,  
 $\epsilon$  is emissivity = 0.985,  
 $b$  is the linear dimension of ice crystals, and  
 $\theta$  is the fractional volume of ice fragments =  $1 - \beta$ .

Substituting in the above expression, the typical values  $\rho_f = 0.13 \text{ g/cc}$  and  $T = 266 \text{ °K}$  (Reference 10) we obtain

$$k_r \leq 1.43 \times 10^{-4} \text{ w/m°C} \quad .$$

However, from Equations (8) and (9) at the same temperature we have,

$$k_i = 2.37 \text{ w/m°C} \quad \text{and} \quad k_a = 0.0236 \text{ w/m°C}.$$

This indicates that the radiation effective conductivity is some two orders of magnitude less than the thermal conductivity of air. In addition, a typical experimental data of frost thermal conductivity appears to show a noise level around  $10^{-3}$  w/m°C or more. Therefore the radiation effective conductivity is considered negligible.

### 2.1.3 Water Vapor Effective Conductivity, $k_v$

The concept of the water vapor effective conductivity is obtained by assuming the energy term,  $L \frac{dm_d}{dx}$ , in Equation (7) obeys the diffusion equation and meets the condition of water vapor saturation in the frost layer. This concept is, of course, invalid when the frost layer becomes supersaturated or subsaturated. Whether these conditions exist or not depends on the significance of nonequilibrium dynamics versus a strong tendency toward an equilibrium state within the frost layer. Since in frost formation whereby the water vapor flux enters the frost layer, the state of subsaturation is quite unlikely. If the water vapor flux into the frost layer is so rapid that homogeneous nucleation occurs, then a state of supersaturation exists (Reference 11). But because there are several nucleation sites within the layer to prevent homogeneous nucleation, one expects there exists a critical wall temperature above which a state of supersaturation is quite unlikely. Experimental evidences of these observations will be shown later.

If the frost layer can be assumed to be in the saturated state, then the water vapor mass flux is given by the following diffusion equation for the frost (Reference 5).

$$\dot{m}_d = \frac{D \beta}{(1-X)\tau_s} \left( \frac{d\rho_v}{dx} \right), \quad (18)$$

where  $D = 1.198 \times 10^{-5} T^{1.75} (P_{atm}/P)$  is the diffusion coefficient (Reference 12 data),

$X$  is the relative concentration (moles  $H_2O$ /moles air),

$\beta$  is the porosity =  $(\rho_i - \rho_f)/(\rho_i - \rho_a)$ ,

$\tau_s$  is the tortuosity, and

$\rho_v$  is the saturated water vapor density (g/cc).

The porosity accounts for the decreased effective cross sectional area for diffusion and the tortuosity, generally taken as 1.1 for frost, accounts for the increased path length the molecules must travel. The assumption (whose verification is apparent later in Figures 2 and 3) that the water vapor at the frost surface is saturated implies that the water vapor mass flux can be made to follow the temperature gradient through the gas law,

$$P_v = \rho_v R_v T \quad , \quad (19)$$

and the Clapyron Equation,

$$P_v = P_v^* \exp \left[ \frac{L}{R_v T^*} - \frac{L}{R_v T} \right] \quad , \quad (20)$$

where  $L$  is the latent heat of ice sublimation or water evaporation (J/g),

$P_v^*$  is the referenced pressure (N/m<sup>2</sup>),

$T^*$  is the referenced temperature (°K),

$R_v$  is the water vapor gas constant = 4.6150 X 10<sup>6</sup> erg/C<sup>2</sup>g,

$\rho_v$  is the water vapor density (g/cc), and

$P_v$  is the water vapor pressure (N/m<sup>2</sup>).

Setting  $L = L_s$ ,  $P_v^* = 610.7$  N/m<sup>2</sup>, and  $T^* = 273$  °K, we obtain,

$$P_v = 610.7 \exp \left( 22.4959 - \frac{L_s}{R_v T} \right) \quad .$$

By differentiating the gas law equation, we obtain,

$$\frac{\partial \rho_v}{\partial x} = \left( \frac{1}{R_v T} \frac{dP_v}{dT} - \frac{P_v}{R_v T^2} \right) \frac{dT}{dx} \quad . \quad (21)$$

The Clapyron equation for  $P_v$  is differentiated with respect to temperature and is substituted along with Equation (21) into Equation (18) to get,

$$\dot{m}_d = \frac{D\beta}{(1-\chi)\tau_s} \left( \frac{P_v}{R_v T^2} \right) \left( \frac{L_s}{R_v T} - 1 \right) \frac{dT}{dx} \quad . \quad (22)$$

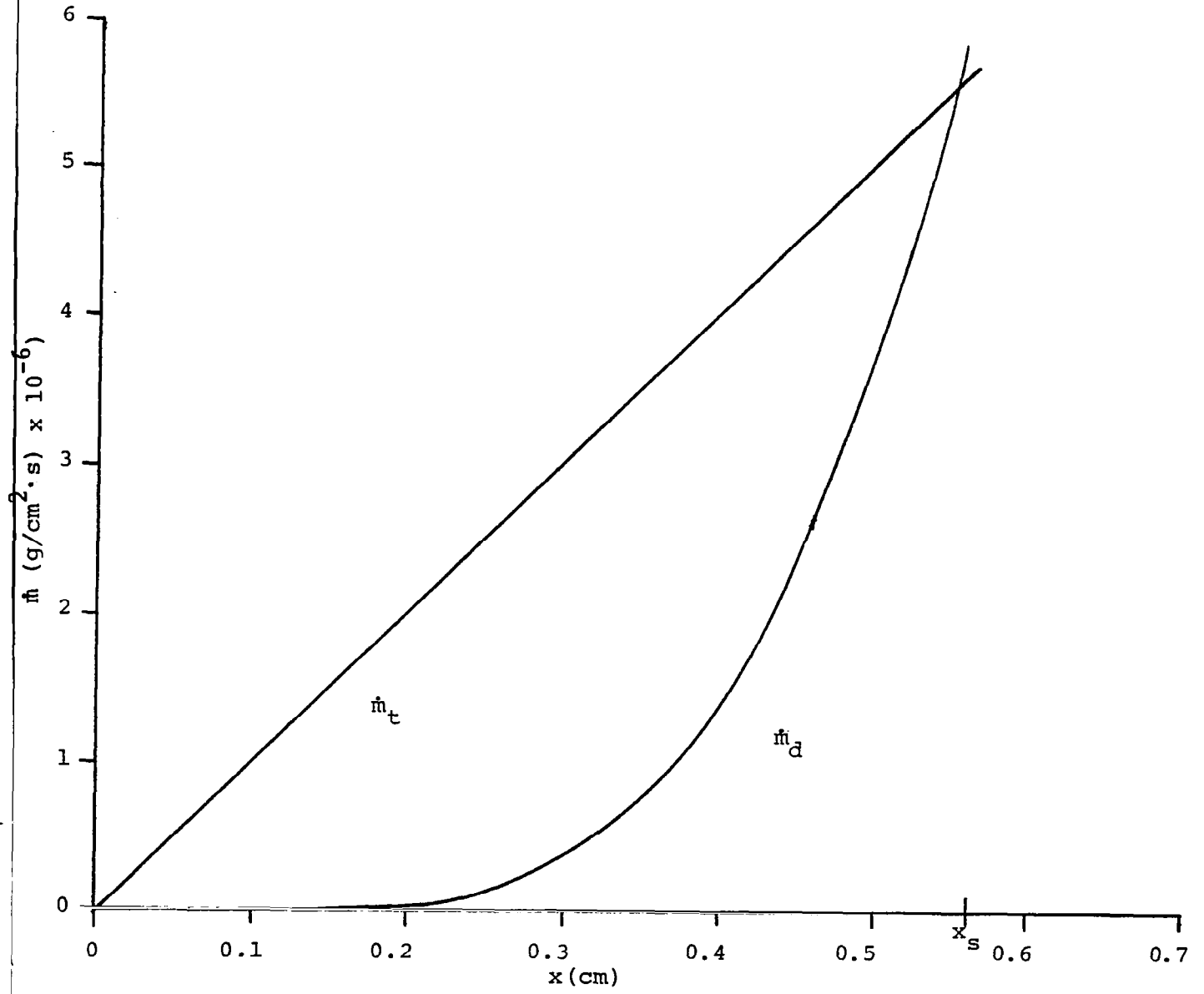


Figure 2. Water mass flux versus distance in frost layer (Brian, et al. data, Reference 1)

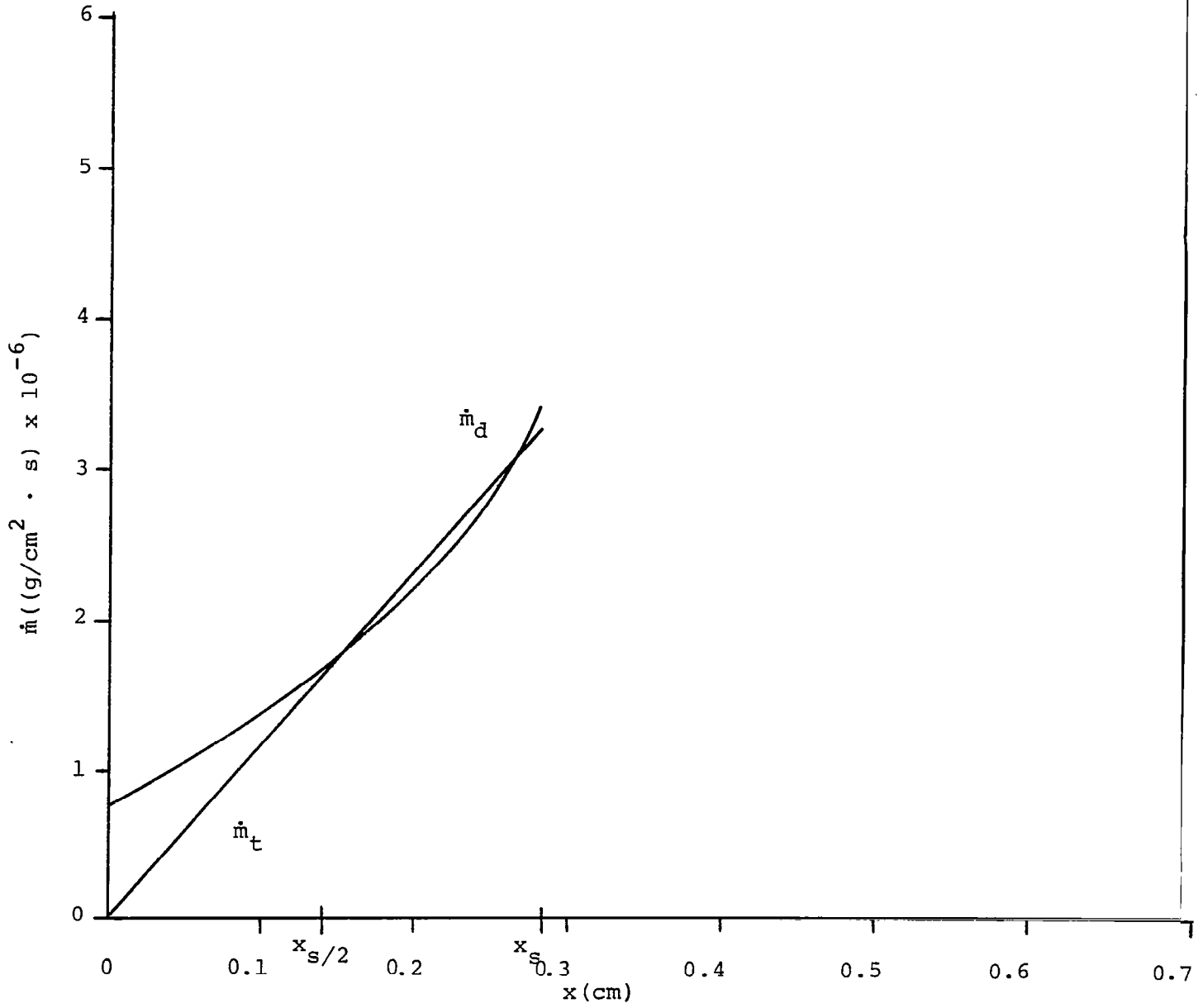


Figure 3. Water mass Flux versus distance in frost layer  
(Yamakawa, et al. data, Reference 13)

Since the water vapor mass flux is now directly related to the temperature gradient, a thermal conductivity due to the water vapor latent heat flux is defined by

$$k_v \equiv \frac{\dot{m}_d L_s}{(dT/dx)} = \frac{L_s D \beta}{(1-\chi) \tau_s} \left( \frac{P_v}{R_v T^2} \right) \left( \frac{L_s}{R_v T} - 1 \right) \quad (23)$$

Equation (23) is seen to be closely linked to the saturation conditions through the term  $(dP_v/dT)/R_v T$  in Equation (21). The second term in Equation (21),  $P_v/R_v T^2$ , was found to be quite small in comparison. If supersaturation exists, then the Clapyron equation is no longer valid and a new equation for  $P_v$  would have to be derived for this state. Fortunately, it was found this is not necessary, as the following experimental evidence will show.

According to Equation (22), if experimental values of the frost density and temperature distribution are known, then the water vapor mass flux can be calculated as a function of the "x" variable as shown in Figure 1 within the frost layer. Observations by several authors (References 1, 2, 3, 13, and 14) indicate that the frost density is nearly spatially invariant in the "x" direction. This means the total water mass flux,  $\dot{m}_t$ , consisting of water vapor and nucleated water drops, is given approximately by,

$$\frac{d\dot{m}_t}{dx} = \frac{\dot{m}_t}{x} = \frac{\dot{m}_{exp}}{x_s} \quad (24)$$

where  $\dot{m}_{exp}$  is the experimentally calculated value of the water mass flux into the frost surface from the surrounding air and  $x_s$  is the frost thickness. If one observes that  $\dot{m}_t \leq \dot{m}_d$  for all values of x, then no nucleated drops have formed; this means a supersaturated state is unlikely. If one observes that  $\dot{m}_t > \dot{m}_d$  for some values of x, then nucleation has occurred, and thus supersaturation might be possible. Note that homogeneous nucleation and nucleation on nucleating sites in the frost layer cannot be experimentally distinguished. Thus we cannot state definitely if supersaturation has occurred. If  $\dot{m}_d = \dot{m}_t$  at the

frost surface or at distance,  $x_s$ , then we have a good method for predicting the frost density growth rate for which a formula will be derived in Section 4.

Figure 2 shows a plot of  $\dot{m}_d$  and  $\dot{m}_t$  calculated from an experimental run of Brian, et al. (Reference 1), where the wall temperature was at 80°K. The steep rise of the  $\dot{m}_d$  curve is due to the temperature dependent relationship of  $D$  and  $P_v$  in Equation (22) for the temperature increase from 80°K to about 265°K. In comparison to the  $\dot{m}_t$  curve it is probable that some supersaturation has occurred, given the magnitude of the difference between  $\dot{m}_t$  and  $\dot{m}_d$ . At distance  $x_s$  from the wall we note that  $\dot{m}_d$  is equal to  $\dot{m}_t$ . A data set with a more reasonable temperature range applicable for frost formation on an aircraft can be obtained from Yamakawa, et al. (Reference 13). Here the range of temperature, in one specific case, is from -22°C to -3.3°C. Although the experimental temperature distribution within the frost is not available, indications are that for this small temperature range, the temperature profile can be roughly approximated as a linear function of  $x$ . Thus, the temperature gradient for Equation (22) is given by

$$\frac{dT}{dx} \approx \frac{T_s - T_w}{x_s} = 66.78 \text{ } ^\circ\text{K/cm} \quad , \quad (25)$$

as obtained from experimental data in Reference 13; where  $x_s = 0.28$  cm. At this frost thickness the frost density is 0.1110 g/cc and the ambient absolute humidity is 0.0049 as obtained from the data. Substituting these values into Equation (22) gives the  $\dot{m}_d$  curve shown in Figure 3. For the top half of the frost layer, the  $\dot{m}_d$  curve agrees closely with the  $\dot{m}_t$  curve calculated from experimental data. While for the lower half of the frost layer,  $\dot{m}_d$  is greater than  $\dot{m}_t$ . These observations mean that down to a wall temperature of -22°C we can confidently say the frost layer is in a saturated state. In addition, at the distance  $x_s$ , we find that  $\dot{m}_d \approx \dot{m}_t$ . The conclusion is that the water vapor thermal conductivity is valid for most frost formation situations and an accurate method for calculating the water mass flux entering the frost surface has been obtained.

Now  $k_v$  can be compared directly with  $k_a$  and  $k_i$  for an order of magnitude analysis. From Reference 10, with the same data used in evaluating the radiation effective conductivity, we obtain at the frost surface, with equation (23),

$$k_v = 0.0111 \text{ w/m}^\circ\text{C} \quad . \quad (26)$$

But since  $k_a = 0.0236 \text{ w/m}^\circ\text{C}$ , the water vapor thermal conductivity cannot be ignored at low frost density. At higher frost density,  $k_v$  actually decreases due to the porosity term in Equation (23). At close to ice density the term  $k_i = 2.37 \text{ w/m}^\circ\text{C}$  indicates the dominating influence of  $k_e$ . So far, the order of magnitude calculations show that particular attention must be devoted to developing the air-ice thermal conductivity which would include a complicated frost structure modeling and perhaps also the water vapor thermal conductivity at low frost density.

#### 2.1.4 Forced-Air Enthalpy Rate Term, $G_a C_p \frac{\partial T}{\partial x}$

The air mass flux,  $G_a$ , is difficult to determine because it is strongly dependent on the frost structure. If the frost structure consists primarily of ice cylinders that penetrate deeply into the ambient flow of air, then perhaps  $G_a$  can be approximated conservatively to the upper limit, e.g.,  $\rho_a V_\infty$ . But that situation is unlikely since, as shown above, the frost structure is not simple. That is, the initial frost may form ice trees, but the frost thickness is so thin that it barely penetrates the momentum boundary layer. This means the velocity,  $v_a$ , is some small fraction of the free stream velocity. As the frost thickens, the frost density will also increase, causing a close knit mesh of ice dendrites. This frost structure would eliminate any forced-air flow through the frost. It is noted the wall is impermeable, so there is no suction or blowing underneath the frost layer. In the study of heat and mass transfer coefficients in Section 3, for the forced convection case, we show that the effective frost surface area for the turbulent heat transfer coefficient remains a constant for all values of the frost density and thickness. But for the laminar,

natural convection case, there is no frost surface effect on the heat transfer coefficient. Thus it is concluded that the momentum boundary layer begins at the frost surface for the laminar natural convection case and begins at some constant minute distance below the frost surface in the turbulent forced convection case. In this situation, the only mass flux within the frost layer is the total water flux,  $\dot{m}_t$ , which is set equal to  $G_a$ .

Consequently from Brian data, as also used to evaluate  $k_v$  and  $k_r$ , a high estimate is made of the forced-air enthalpy rate term in Equation (7) for comparison with the  $\dot{m}_d$  term by using the measured temperature gradient for the water vapor mass flux at the frost surface. The result is,

$$\dot{m}_{d_s} C_a \left. \frac{dT}{dx} \right|_s = 8.44 \times 10^{-4} \text{ w/cc.} \quad (27)$$

This can be compared to a low estimate of the latent heat contribution calculated by setting

$$\frac{d\dot{m}_d}{dx} = \frac{\dot{m}_{d_s}}{x_s} \quad (28)$$

in Equation (7) to get

$$\frac{\dot{m}_{d_s} L_s}{x_s} = 2.91 \times 10^{-2} \text{ w/cc.} \quad (29)$$

Comparable results were also obtained within the frost layer. Therefore the heat transfer rate by the forced-air enthalpy rate is much lower than the latent heat release rate within the frost layer. In fact it also appears that the heat transfer by radiation within the frost layer is of the same order of magnitude as the heat transfer by an enthalpy change due to the water vapor flux. Since the experimental data is not accurate to four significant digits as would be required both by the forced-air enthalpy rate and the radiation heat rate, the

terms for the conductive heat rate and the latent heat release rate are only retained in Equation (7) The result is

$$\frac{d}{dx} \left[ k_e \frac{dT}{dx} \right] = -L \frac{d\dot{m}_d}{dx} \quad (30)$$

An expression for a frost thermal conductivity can be derived if Equation (23) is used and substituted in the above equation and integrated. Thus,

$$K \frac{dT}{dx} = q_o \quad ; \quad (31)$$

with 
$$K = k_e + k_v \quad , \quad (32)$$

where  $q_o$  is a constant heat flux at the wall and  $K$  is the thermal conductivity of frost. With the simplified equations above, all other approaches obtained from the literature for calculating the frost thermal conductivity can be explained.

## 2.2 APPROACHES FOR CALCULATING K

### 2.2.1 Brian, et al. Approach

If the heat flux and the temperature gradient are measured, as was done in the frost experiments by Shah (Reference 2) and Brian, et al. (Reference 1), a frost thermal conductivity can be calculated easily from the above equations. It is important that the heat flux should be measured at the wall as is done by Shah (Reference 2) as well as by Brian, et al. (Reference 1) rather than at the frost surface. The reason is because, due to the latent heat contribution, the heat flux becomes lower at the frost surface than at the wall.

Some empirical expressions for the thermal conductivity of frost, based on the experimental data by Shah (Reference 2), Brazinsky (Reference 15), and Brian, et al. (Reference 1), as developed by Brian, et al. (Reference 10) in SI units are

$$K_1 = 2.405 \times 10^{-5} T^{1.272} + 3.931 \times 10^{-5} \rho_f T^{1.74} \quad (33)$$

where  $\rho_f < 0.025$  g/cc and  $T < 255^\circ$  K;

$$K_2 = 3.595 \times 10^{-15} T^{5.44} + 2.042 \times 10^{-12} (\rho_f - 0.025) T^{4.84}, \quad (34)$$

where  $\rho_f > 0.025$  g/cc and  $T \geq 255^\circ$  K; and

$$K_3 = 1.564 \times 10^{-5} T^{1.441} + 4.252 \times 10^{-8} (\rho_f - 0.025) T^{3.055}, \quad (35)$$

where  $\rho_f > 0.025$  g/cc and  $T < 255^\circ$  K and

where  $\rho_f$  stands for the average density of the frost. It may be noted that this empirically developed thermal conductivity is a linear function of the frost density. Later on it will be shown that this relationship is valid only within the experimental range of frost density up to 0.13 g/cc.

Serious problems are encountered if one attempts to use the above type expression for thermal conductivity with other data. This is because a number of factors such as the thermal conductivities of water vapor, air, ice, and the frost structures, which play important parts in the expression for the thermal conductivity of the frost, have not been considered in the above model.

### 2.2.2 White's Approach

Another approach to determine the frost thermal conductivity developed by White (Reference 4) using the empirical relations to fit the Shah data (Reference 2) where  $k_v$  of Equation 32 is given by

$$k_v = \frac{D_{eff} L_s^2 P_v}{R_v^2 T^3}, \text{ and} \quad (36)$$

$$k_e = (0.1684 + 35.39 \rho_f / \rho_{water}) \times (-0.01356 + 0.0001579T), \quad (37)$$

and

where  $D_{\text{eff}} = 100 \text{ mm}^2/\text{sec}$ . Although this approach is more theoretical than that of Brian, et al., since it takes into account more variables, it is still hampered by the fact that  $k_v$  and  $k_e$  are treated as empirical terms. Another problem is that this approach is valid only in the experimental range of Shah's data (Reference 2) which is  $\rho_f \leq 0.13 \text{ g/cc}$ .

### 2.2.3 Biguria and Wenzel's Approach

Since the water vapor diffusion occurs only in the air portion of the frost, Biguria and Wenzel (Reference 3) suggest that if the effective air thermal conductivity instead of the true air thermal conductivity is used, one can expect better results. The effective air thermal conductivity can be obtained from the relation

$$k_{\text{eff air}} = k_a + \frac{DP_t}{P_t - P_v} \left( \frac{L_s P_v}{R_v T^2} \right) \left( \frac{L_s}{R_v T} - 1 \right) = k_a + \frac{\tau_s k_v}{\beta} \quad (38)$$

which is based on Equation (21) of Reference 3 and Equation (23). It may be noted that for obtaining the air effective conductivity, the tortuosity and the porosity expressions in the vapor effective conductivity are neglected as they have no use as corrections in the air portion of the frost. According to Biguria and Wenzel (Reference 3) one can obtain a better expression for  $k_e$  by using  $k_{\text{eff air}}$  instead of  $k_a$  in Equations (10) to (16). For frost densities greater than 0.05 g/cc, Biguria and Wenzel claimed that a good fit to their experimental data was obtained by using this approach and Equations (15) or (16). The experimental thermal conductivity of frost was obtained, however, by measuring the heat flux at the wall, the thickness of the frost, and the wall and frost surface temperatures. In order to apply the theoretical thermal conductivity equations to the data, Biguria and Wenzel implicitly assumed the frost layer has uniform temperature,

structural, and density distributions. These assumptions require the wall temperature to be a high temperature at around 250° K, the frost to be formed in a specified structure, and the ambient absolute humidity to be in a specified range near saturation. In contrast, the data of Brian, et al. (Reference 1) and Shah (Reference 2) typically has the wall temperature at 80° K, more spherical ice formations than ice trees, and an ambient absolute humidity at a fraction of the saturation level. Thus it is expected the approach by Biguria and Wenzel will not fit satisfactorily to the data of Brian, et al. (Reference 1) and Shah (Reference 2). This actually turned out to be the case. The basic disadvantage in this approach is the requirement of a uniform temperature and structural distribution of the frost.

#### 2.2.4 Jones and Parker's Approach

By assuming that the frost density is spatially invariant so that the amount of water vapor being frozen is the same at all locations in the frost layer, the change in the vapor mass flux with distance is

$$\frac{d\dot{m}_d}{dx} = \frac{\dot{m}_{d_s}}{x_s} , \quad (28)$$

where  $\dot{m}_{d_s}$  is the water vapor flux driven by the temperature gradient at the frost surface. Jones and Parker (Reference 5) have used this relationship to model the heat transfer mechanism in the frost layer, and thus also the model of the frost thermal conductivity. Substituting the above expression into Equation (30) and integrating, we get,

$$k_e \frac{dT}{dx} = \frac{-L_s \dot{m}_{d_s}}{x_s} x + q_o , \quad (39)$$

where

$$q_o = h_H (T_a - T_s) + h_m L_s (\omega_a - \omega_s) \quad (w/m^2) ,$$

$h_H$  is the heat transfer coefficient ( $w/m^2 \text{ } ^\circ C$ ),  
 $h_m$  is the mass transfer coefficient ( $g/m^2 \text{ sec } ^\circ C$ ),  
 $T_a$  is the ambient air temperature ( $^\circ K$ ),  
 $T_s$  is the frost surface temperature ( $^\circ K$ ),  
 $\omega_a$  is the absolute ambient humidity, and  
 $\omega_s$  is the frost surface humidity.

It may be noted here,  $k_e$ , which is computed in the usual way as in Equations (10) to (16), does not contain the expression for  $k_{\text{eff air}}$ . Also, Jones and Parker (Reference 5) used the incorrect expression for  $k_e$  by using Brian, et al.'s (Reference 1) empirical frost thermal conductivity. This approach has two difficulties. If a linear vapor mass flux with distance which releases the latent heat is assumed, then, because of what has been shown in Figures 2 and 3, a supersaturated state would have to exist in Brian, et al.'s data (Reference 1) and a subsaturated state would have to exist in Yamakawa's data (Reference 13) within the frost layer. This dual state is physically unlikely, especially if several ice crystals also exist along side of the moist air within the frost layer. The second difficulty is that this approach cannot be compared with experimental data unless the term  $\dot{m}_d$  can be calculated from each data set. Usually the values of  $\dot{m}_d^s$  are absent in the literature available.

#### 2.2.5 Summary of the Four Approaches

If one examines carefully the aforementioned approaches which have been established on the basis of a controlled environment, one will find that they are not satisfactory for the aircraft frost formation problem where the environmental variables have different ranges. The validity of the first approach, given by Brian, et al. (Reference 1), is restricted to frost densities less than 0.13 g/cc and very low wall temperatures and ambient humidities, as indicated in Table 1. If the empirical frost thermal conductivities based on ice density are extrapolated, the sharp disagreement with the actual thermal conductivity of ice is apparent in Figure 4. Similarly, if the same is done on the basis of air density, the resulting curves in Figure 5 show the disagreement with the actual thermal conductivity of the air. It may be noted that the effective conductivity of water vapor, which becomes negligible for temperatures less than 225° K due to the rapid decrease in  $D$  and  $P_v$ , was not considered in the thermal conductivity of air. On the basis of the same arguments,

TABLE I

Summary of Approaches to Calculating  
Frost Thermal Conductivity

Approach	Range of Application	Modeling Technique	Modeling of the Frost Structure	Limitations
Brian, et al. (Reference 1)	$\rho_f < .13\text{g/cc}$ $T_w = 80^\circ \text{K}$	Empirical	None	Average Thermal conductivity will not fit data at other wall temperatures.
White (Reference 4)	$\rho_f < .13\text{g/cc}$ $T_w = 80^\circ \text{K}$	Semi-empirical	Vapor diffusion in frost layer is postulated	Same as Brian, et al. (Reference 1)
Biguria & Wengel (Reference 3)	$.05\text{g/cc} < \rho_f < \rho_{\text{ice}}$ $T_w > 250^\circ \text{K}$	Theoretical	Simple Frost structures is postulated	Same as Brian, et al. (Reference 1)
Jones & Parker (Reference 5)	$\rho_f < .13\text{g/cc}$	Semi-empirical	Vapor diffusion in frost layer is postulated	Super saturation within frost layers is unlikely.
UDRI Approach	$\rho_a < \rho_f < \rho_{\text{ice}}$ $80^\circ \text{K} < T_w < 265^\circ \text{K}$	Mostly theoretical partly empirical	Complicated frost structure is postulated for vapor diffusion, geometrical shapes of ice dendrites, and for frost aging.	

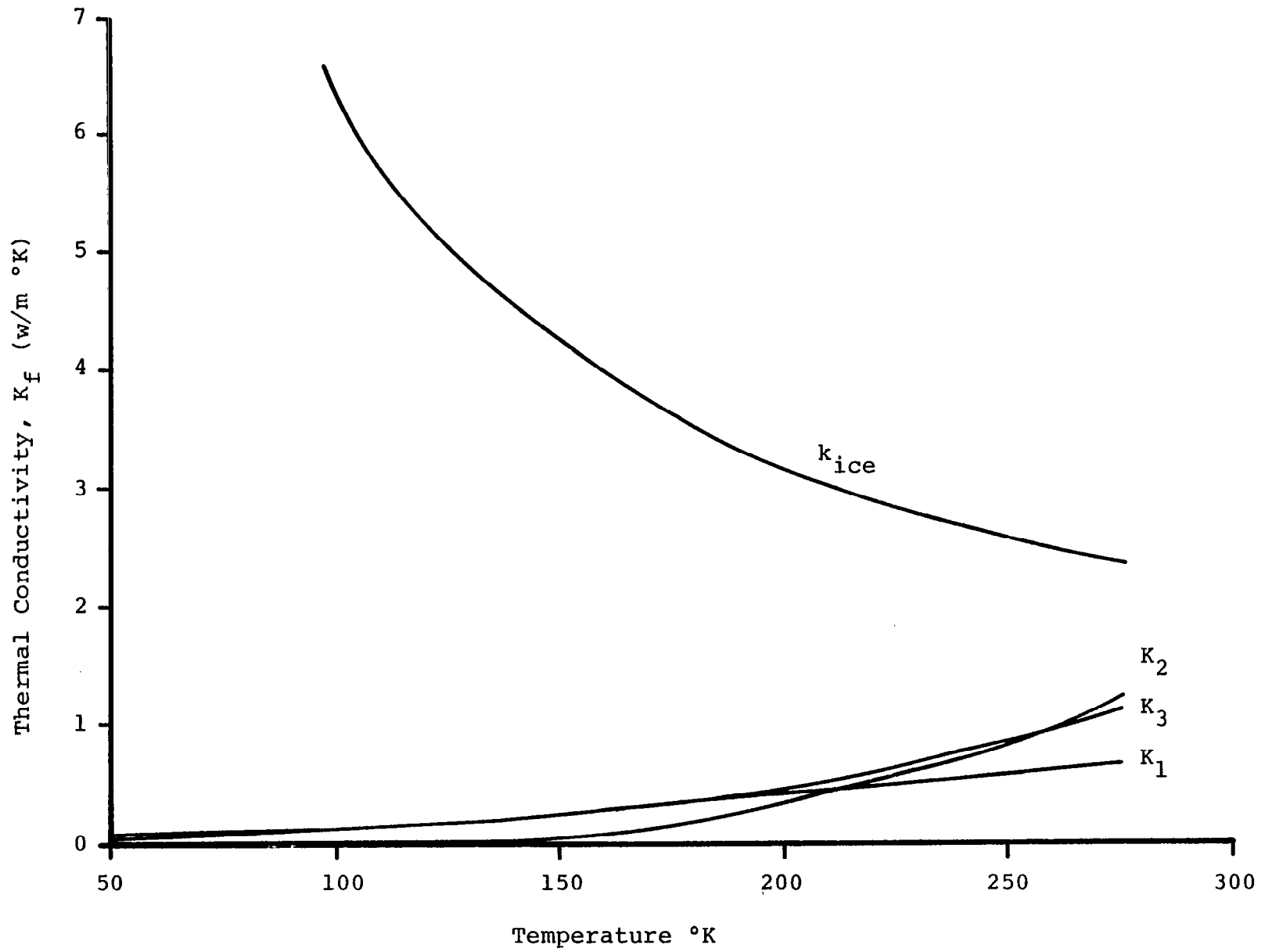


Figure 4: Thermal conductivity versus temperature at ice density

2-22

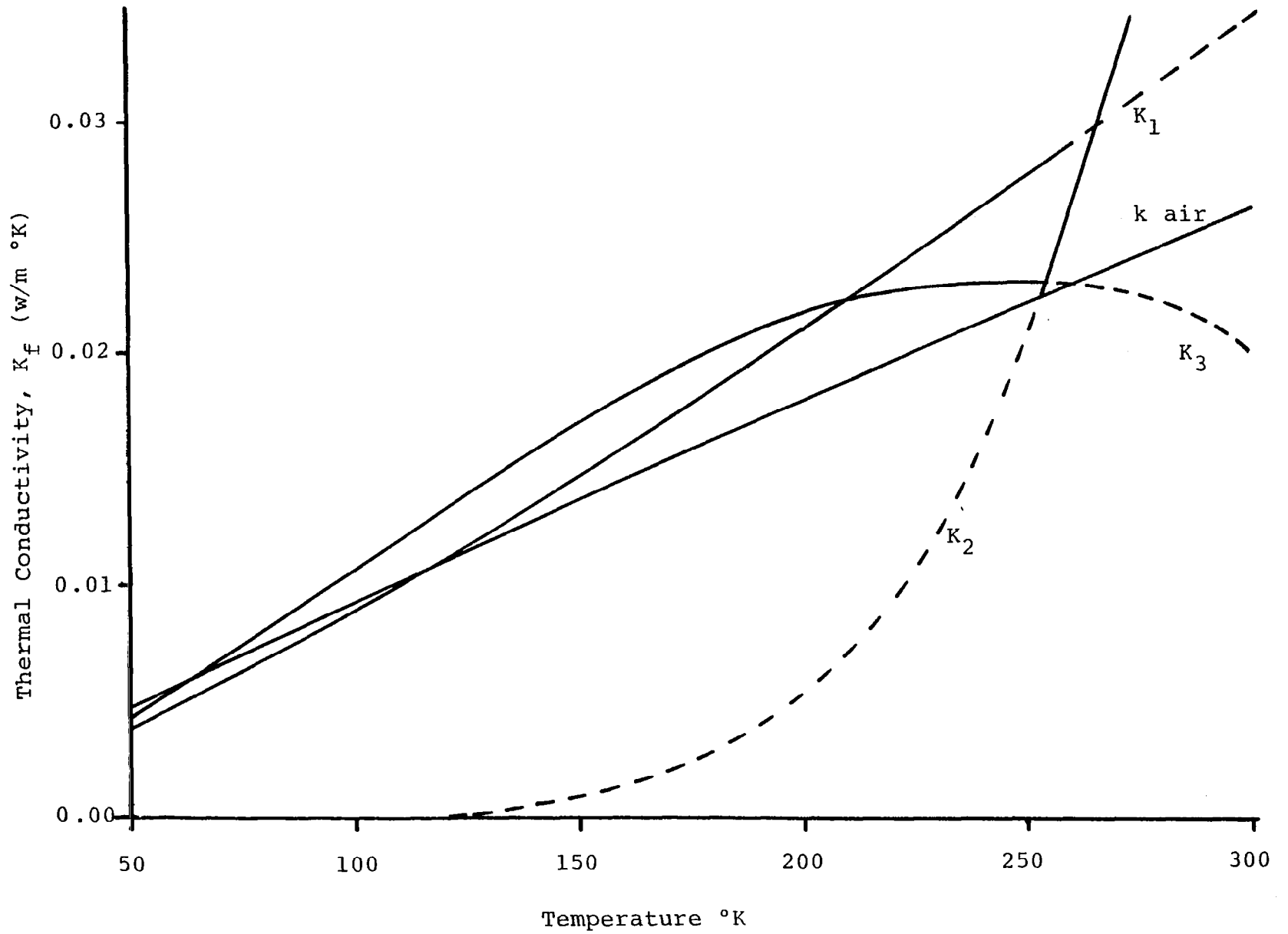


Figure 5: Thermal conductivity versus temperature at air density

the approach given by White (Reference 4) is found unsatisfactory for our problem. Since the state of super- or subsaturation within the frost layer is unlikely to exist, Jones and Parker's approach (Reference 5) is not being used in our analysis. When the available experimental data could not be fitted to the theoretical approach suggested by Biguria and Wenzel (Reference 3), an attempt was made to see if the experimental values of frost thermal conductivity given by Brian, et al. (Reference 1) could lie between the curves represented respectively by Equations (13) and (14) for either spherical air pores or spherical ice particles. The encouraging results in Figure 6 showed that the frost thermal conductivity is a linear function of porosity or frost density for porosities greater than 0.85. This gave a motivation to propose a new model, based on Biguria and Wenzel's theoretical approach (Reference 3), but which includes frost structure parameters which could be empirically derived to fit Brian, et al.'s data (Reference 1), as well as other data.

#### 2.2.6 The UDRI Approach

The proposed model makes the following assumptions about the frost structure as shown in Figure 7. At low frost density, or at high porosity, two types of frost structure predominate. One is the ice cylinders created by the internal diffusion of water onto the ice, which result in a parallel conductive heat transfer. The other portion is the ice spheres created by nucleation of water vapor, resulting in a much lower conductive heat transfer. The total structure of the frost is then the random mixture of ice cylinders and ice spheres (Figure 7a). At high frost density, or low porosities, completely different dual structures begin to take shape. In contrast to the low density case, spherical air voids are formed in place of ice cylinders (Figure 7b). This results in enhanced thermal conduction. Also, in place of the ice spheres, stratified layers are formed. The total frost structure is then a random mixture of air bubbles and ice layers.

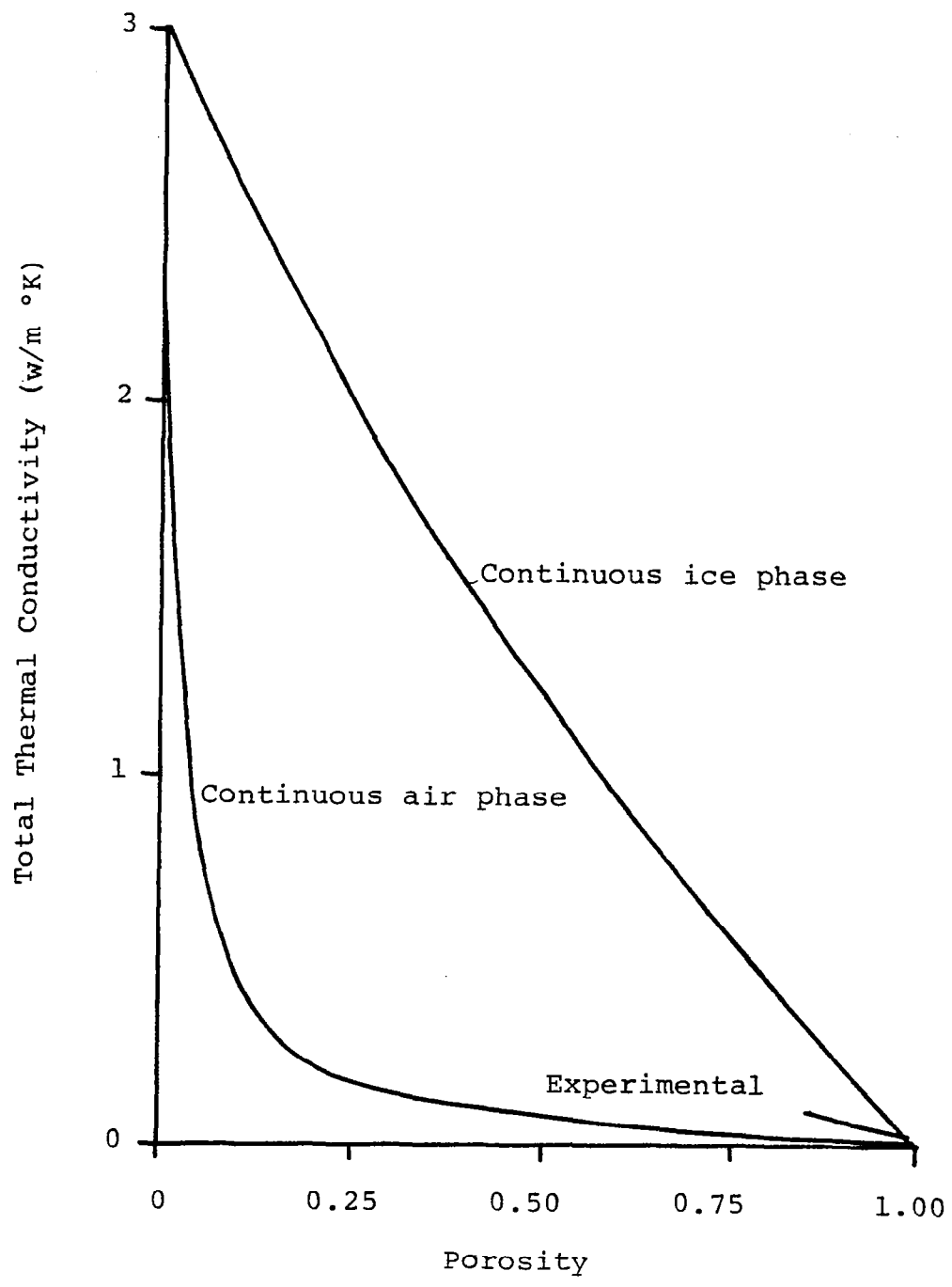
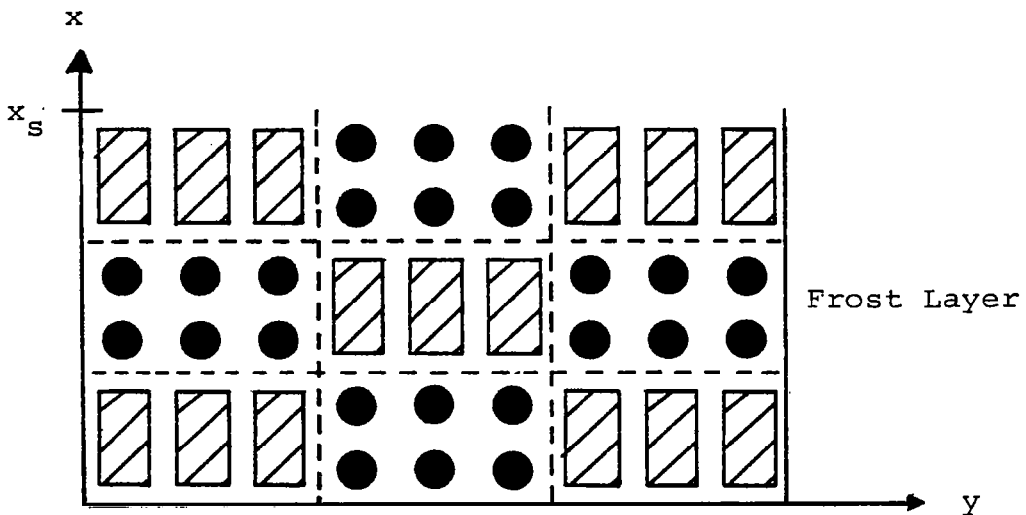
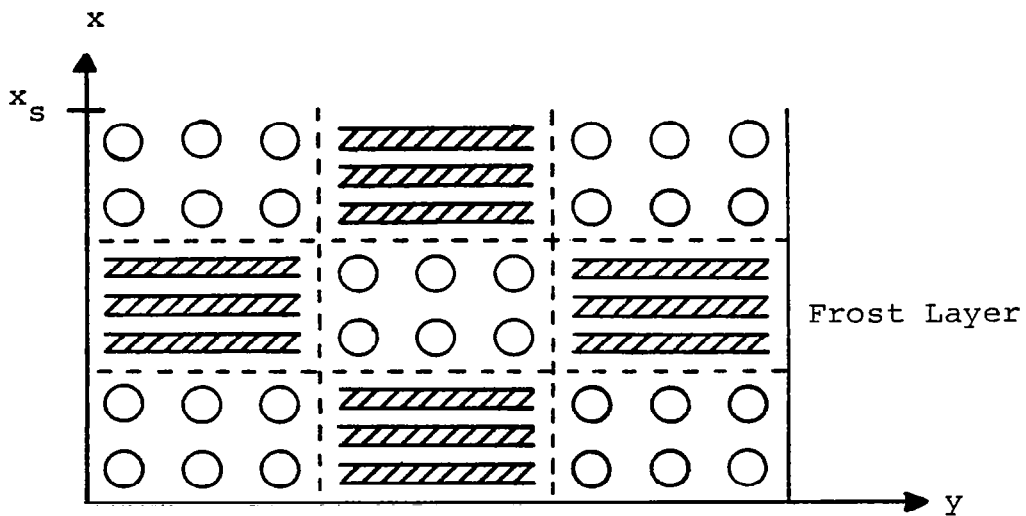


Figure 6: Thermal conductivity versus frost porosity at 211 °K



Random mixture of ice cylinders and ice spheres  
at high porosities or low frost densities

(a)



Random mixture of ice planes and air bubbles  
at low porosities or high frost densities

(b)

Figure 7. Frost Structure Model of the present work

With such a model of the frost structure, the equations for air-ice thermal conductivity presented earlier are combined in two ways. First, an attempt was made to arrive at the upper limit and the lower limit of thermal conductivity as a function of porosity. The second part attempts to ascertain the combined contribution of the upper limit and the lower limit of the thermal conductivity to the frost thermal conductivity as a function of temperature. Noting that the thermal conductivities for ice cylinders and for air bubbles are close to each other for all porosities, a simple interpolation rule is used to obtain the upper limit of the thermal conductivity.

$$k_u = (1-\beta) k_b + \beta k_c \quad (\text{upper limit}), \quad (40)$$

$$k_b = k_i \left[ 1 - 2\beta \left( \frac{1-\alpha}{2+\alpha} \right) \right] / \left[ 1 + \beta \left( \frac{1-\alpha}{2+\alpha} \right) \right] \quad (\text{air bubbles}), \quad (13)$$

$$k_c = (1-\beta) k_i + \beta k_{\text{eff air}} \quad (\text{ice cylinders}), \quad (11)$$

$$\alpha = k_{\text{eff air}} / k_i \quad .$$

Likewise, the lower limit of thermal conductivity is formed by an interpolation between thermal conductivities for ice spheres and ice planes.

$$k_l = (1-\beta) k_p + \beta k_s \quad (\text{lower limit}) \quad (41)$$

$$k_s = k_i \left[ 3 + 2\beta(\alpha - 1) \right] / \left[ 3 - \beta \left( \frac{\alpha - 1}{\alpha} \right) \right] \quad (\text{ice spheres}), \quad (14)$$

$$k_p = \frac{k_i k_{\text{eff air}}}{(1-\beta) k_{\text{eff air}} + k_i \beta} \quad (\text{ice planes}). \quad (10)$$

To determine the combined contribution of the upper and the lower limits of the thermal conductivity to the frost thermal conductivity, the random mixture model of Brailsford and Major given by Equation (15) is utilized. The present model of thermal conductivity of frost given as

$$K = 1/4 \left\{ \left( (3\beta_c - 1) k_l + (3\theta_c - 1) k_u + \left[ \left( (3\beta_c - 1) k_l + (3\theta_c - 1) k_u \right)^2 + 8k_l k_u \right]^{1/2} \right) \right\} \quad (42)$$

is used to combine  $k_l$ ,  $k_u$ , and  $\theta_c$ . The proportion of the frost volume,  $\beta_c$ , representing ice spheres and ice planes given as a parabolic function of the porosity  $\beta$  is

$$\beta_c = a + b\beta + c\beta^2, \quad (43)$$

where  $a$ ,  $b$ , and  $c$  can be constant or functions of temperature. The other portion of the frost volume representing ice cylinders and air bubbles is given by

$$\theta_c = 1 - \beta_c, \quad (44)$$

It is plausible to assume the frost takes on a completely spherical air voids structure when the porosity in the frost approaches zero or the density of the frost approaches that of ice. This assumption when translated into boundary condition for Equation (43), gives  $\beta_c = 0$  for  $\beta = 0$  and thereby 'a' is found to be zero. Another plausible assumption is that all frost structures converge to the same structure as the porosity approaches zero regardless of the frost temperature. It gives 'b' as a constant and 'c' will then be a strong function of temperature. Since each curve in Figure 8 is at a different temperature, it is possible to determine the values of 'b' and 'c' from it. The result indicates that 'b' is indeed a constant and 'c' is a function of local temperature of the frost, hence the value of  $\beta_c$  becomes

$$\beta_c = \beta \left\{ 0.9 + \left[ 0.1 + \frac{80^2 - T^2}{(357)^2} \right] \beta \right\}. \quad (45)$$

As shown in Figure 8, it gives a multiple correlation of 0.99 and a standard deviation to the third decimal place as a fit to Brian, et al.'s data (Reference 1). In order to compare the frost conductivity, as predicted from the proposed model, to other experimental data, an average frost thermal conductivity is needed. The average frost thermal conductivity, denoted by  $\bar{K}$ , is defined as

$$\bar{K} = \frac{\int_{T_w}^{T_s} K dT}{T_s - T_w} \quad (46)$$

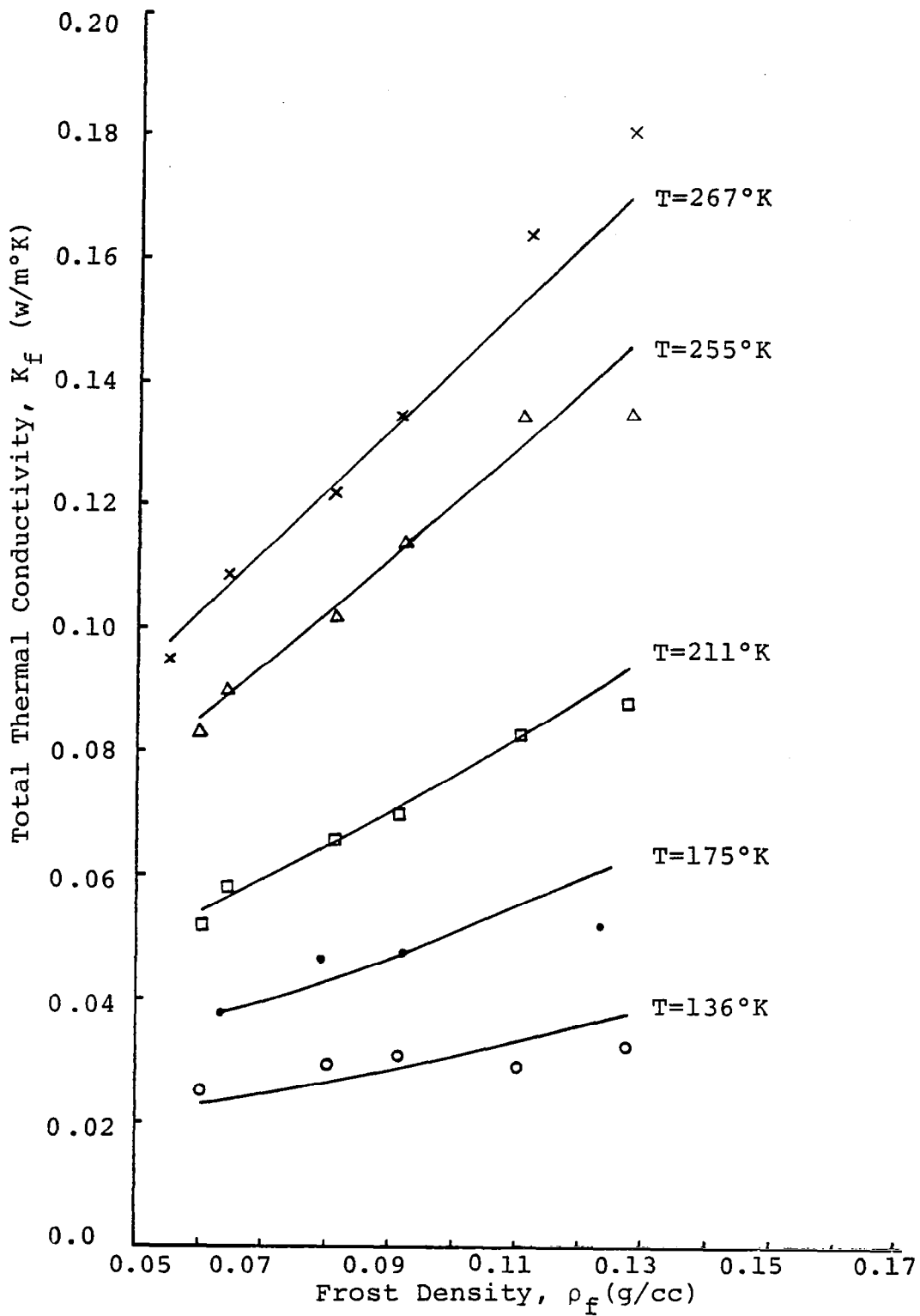


Figure 8. Comparison of the Present Frost Thermal Conductivity Model with Experimental Data of Brian, et al. (Reference 1)

where  $T_s$  is the frost surface temperature and  $T_w$  is the wall temperature. The calculated value of  $\bar{K}$  agreed excellently with Brian, et al.'s data (Reference 1). But Yamakawa, et al. (Reference 13) and Nakamura's data (Reference 14) gave biased values on the low side for  $\bar{K}$ . The reasons for the discrepancy seem to be the following. The effects of frost aging and the size of the water droplets arriving at the frost surface cause the formation of various types of frost structures. In Brian, et al. data (Reference 1), where

$$T_w = 80^\circ \text{ K and } \phi_a \approx 20\%, \quad (47)$$

the extremely low temperature coupled with low relative humidities is found to cause the formation of several large size water droplets, which may freeze instantaneously on the wall. This conclusion was derived from Rosner and Epstein (Reference 11) in the case of fog formation near cold surfaces. As the frost surface temperature increases with time, the smaller water droplets arrive at the frost surface and due to sharp temperature gradient, nucleation takes place within the frost layer. Also, as the frost density increases, the ice dendrites begin to mesh together. These effects are due to the aging of the frost and are aptly included in the empirical relationship for  $\beta_c$ .

On the other hand, in Yamakawa, et al. (Reference 13) and Nakamura (Reference 14) data where  $T_w = 245^\circ \text{ K}$  and  $\phi_a \approx 40\%$  to  $90\%$ , the much higher wall temperature coupled with higher ambient humidities are expected to cause the formation of smaller water droplets which would not freeze instantaneously on the wall. Therefore, initially, the value of  $\beta_c$  for their data should be lower than that of Brian, et al. data (Reference 1), as the presence of the spherical ice particles in the frost layer is less probable. In this case, the water droplets tend to remain at the same size and due to the higher wall temperature, nucleation within the frost layer is not probable, even though the frost surface temperature increases with time. Due to the foregoing reasoning, it is apparent that the expression for  $\beta_c$  should also include

the effect of wall temperature and the effect of the aging of frost. On the basis of the reasons given above, and for preliminary studies on frost formation, the expression for  $\beta_c$  is proposed as

$$\beta_c = \beta \left\{ .9 + \left[ .1 + \frac{80^2 - T^2}{(.526T_w + 315)^2} \right] \beta \right\} \quad (48)$$

When the proposed Equation (48) is used for calculating the average thermal conductivity of the frost at  $T_w$  around 250°K, the results show a good agreement with the data by Yamakawa, et al. (Reference 13) and Nakamura (Reference 14). It may also be noted that at  $T_w = 80^\circ\text{K}$ , Equation (48) reduces to Equation (45) which gives excellent agreement for the data by Brian, et al. (Reference 1). Thus the expression for thermal conductivity with  $\beta_c$  given by Equation (48) is used for the present frost formation model and the results are discussed in the last section of this report.

### SECTION 3

#### HEAT AND MASS TRANSFER COEFFICIENTS

The diffusion of water vapor from the moist air across the frost surface and then into the interior of the frost layer is the mechanism by which the frost layer grows. The rate of growth will be determined by the rate of this mass transfer and the rate of heat transfer to and from the frost layer. To quantitatively predict the growth of the frost, the rates of mass and heat transfer across the frost surface plane shown in Figure 1, must be determined. As in other heat and mass transfer problems it is convenient to represent these convective transfer rates as a heat or mass transfer coefficient multiplied by a suitable potential difference, either temperature,  $T$ , or concentration,  $\omega$ , as appropriate. That is,  $q_o = h_H(T_a - T_s)$ , and  $\dot{m}_t = h_m(\omega_a - \omega_s)$ . This section deals with the several methods of representing the heat and mass transfer coefficients that have appeared in the literature. These coefficients are analyzed and compared with the experimental data available. The poor comparisons obtained indicated that modified coefficients were needed and consequently are developed in this section.

Because of the limited availability of data, the heat and mass transfer coefficients could only be compared at two extreme experimental conditions. The first condition is the frost formation on a vertical wall under laminar natural convection. The other condition is the frost formation in a horizontal duct under turbulent forced convection. Therefore, only the heat and mass transfer coefficients for these conditions are examined. Heat and mass transfer processes for other conditions, such as the airfoil geometry, are not examined because no experimental data is available for comparison. By analyzing for the two extreme experimental conditions two tasks can be accomplished. The first is that the heat and mass transfer processes for the other conditions can be inferred, and secondly, the frost formation model can be severely tested for accuracy under the extreme conditions.

Because accurate transfer coefficients for the frost structure are not available in the literature some investigators have tried to use empirical correlations such as are used in other convective heat transfer problems. Two of these for turbulent forced convection in a duct are the Colburn equation (Reference 16),

$$\text{StPr}^{2/3} = 0.023 \text{ Re}^{-0.2}$$

$$\text{or } \text{Nu} = 0.023 \text{ Re}^{0.8} \text{ Pr}^{1/3} = h_H L / k_a, \quad (49)$$

where Nu, Pr, Re and St stand respectively for the non-dimension Nusselt, Prandtl, Reynolds and Stanton number, and the Dittus - Boelter equation (Reference 16)

$$\text{Nu} = 0.023 \text{ Re}^{0.8} \text{ Pr}^{0.4} \quad . \quad (50)$$

Once the heat transfer coefficient is known, some methods are available to find the mass transfer coefficients under forced convection (Reference 6),

$$h_H / h_m = C_p \quad , \quad (51)$$

and the Chilton - Colburn analogy (Reference 6)

$$h_H / h_m = C_p \text{ Le}^{-2/3} \quad , \quad (52)$$

where  $C_p$  is specific heat of air (J/g °K),  
 $h_H$  is heat transfer coefficient (w/m<sup>2</sup> °C),  
 $h_m$  is mass transfer coefficient (g/m<sup>2</sup>s), and  
 $\text{Le}$  is Lewis number =  $\rho_a C_p D / k_a$  .

These relationships have been slightly modified for special situations. Kays and Perkins (Reference 16) show that for the Prandtl number between 0.5 and 1.0 and a constant wall temperature, the heat transfer coefficient for turbulent forced convection in a duct can be better correlated by the equation

$$\text{Nu} = 0.021 \text{ Re}^{0.8} \text{ Pr}^{0.6} \quad , \quad (53)$$

than by the Colburn equation. For a vertical plate under laminar natural convection, the Nusselt number,  $Nu_z$ , is correlated to the local Grashof number,  $Gr_z$  by the equation (Reference 6)

$$Nu_z = 0.421 Gr_z^{1/4} Pr^{1/2} . \quad (54)$$

To show that these transfer coefficients need modification, the heat transfer coefficient experimentally obtained by Yamakawa, et al. (Reference 13) and Nakamura (Reference 14) were compared with Equations (53) and (54), respectively. Equation (53) when compared to Yamakawa data gave errors biased by about 200%, while Equation (54) compared to Nakamura data gave about a 25% error bias. Further significance of these errors will also be shown in the next section. Other experimentors (References 1, 2 and 4) have attempted to measure the accuracy of the heat and mass transfer processes for frost. Unfortunately, they have not succeeded for all the possible experimental ranges in correlating the experimental data by empirical relations.

To explain the experimental disagreements noted earlier and the difficulties of several experimentors, three postulates are advanced. The first is that the suction or blowing of the water vapor at the frost surface will affect the thermal boundary layer and thus also the heat transfer coefficient. Secondly, fog formation or nucleation in the boundary layer will enhance the water vapor mass transfer and possibly also enhance the heat transfer. Lastly, due to frost porosity, the heat and mass transfer coefficients are affected by the effective area of the frost surface which equivalently can be termed as frost roughness. With these three postulates in hand, the results of Nakamura (Reference 14) and Yamakawa, et al. (Reference 13), are analyzed to determine which of the postulates are significant for a particular experimental condition. Thus the modification of the heat and mass transfer coefficients can be quantitatively described for the two extreme experimental conditions and qualitatively described for all other experimental conditions. With the modified coefficients in hand, the heat and mass fluxes to the frost surface can be calculated.

### 3.1 LAMINAR NATURAL CONVECTION

The results from Nakamura (Reference 14) show that in laminar natural convection on vertical plates the surface roughness has no effect on the heat transfer coefficient because the sensible heat flux from the air to frost is mostly conductive, rather than convective. Also, the nucleation in the boundary layer has only a small effect on the heat and mass transfer coefficients, because the amount of vapor mass flux is usually so small that there is only minute fog formation. However, for natural convection, the momentum, heat and mass transfer mechanisms are coupled together in the boundary layer. The analysis for this problem is taken from Okino and Tajima (Reference 17) for a vertical plate under laminar natural convection. After correcting an algebraic error\* in their analysis, the results are as follows.

$$\text{Nu}_H = \frac{h_H H}{k_a} = \eta / \xi, \quad \text{Sh}_H = \frac{h_m H}{\rho_a D} = \eta (1 + \omega_s) \quad (55), (56)$$

where

$$\eta = \frac{8}{3} \sqrt{\text{Sc} \cdot \phi} \left[ \frac{\text{Gr}_H}{240 \left( \frac{20}{21} + \text{Sc} \phi \right)} \right]^{1/4} \quad (57)$$

$$\text{Gr}_H = \frac{g H^3}{\nu^2} \left[ \frac{\xi |T_a - T_s|}{T_a} + \frac{|\omega_a - \omega_s|}{|.6453 + 2.6453 \omega_a|} \right] \quad (58)$$

$$\xi = \sqrt{\phi^2 + 2 \frac{\text{Sc}}{\text{Pr}} \phi + 1} - \phi \quad (59)$$

$$\phi = \frac{1 + \omega_a}{1 - \omega_s} \quad (60)$$

$\nu$  is kinematic viscosity,  
 $g$  is gravitational acceleration ( $\text{m/s}^2$ ),  
 $H$  is height of plate (m),  
 $\omega_s$  is saturated absolute humidity, and  
 $\text{Sc}$  is Schmidt number.

The Nusselt and Sherwood numbers ( $\text{Nu}_H$  and  $\text{Sh}_H$ ) by these equations fitted Nakamura's data (Reference 14) quite well.

\*The algebraic error is that the term  $\sqrt{\text{Sc}}$  in  $\eta$  was placed in the denominator instead of the numerator of equation (57) above.

### 3.2 TURBULENT FORCED CONVECTION

In the case of forced convection however, the mass transfer has only a minor effect on the heat transfer coefficient. This is shown as follows. A conservative estimate of the blowing parameter based on Yamakawa, et al. data (Reference 13) gives

$$F = \frac{\dot{m}_t}{\rho_a U_a} = .00002 \quad (61)$$

which, according to a graph presented by Rohsenow and Hartnett (Reference 6), is so small that the exponent of the Reynolds number in Equation (53) remains constant at 0.8. A cursory look at Yamakawa's Nusselt number (Reference 13) versus Reynolds' number plot in Figure 9 verifies this conclusion, which is in opposition to a conclusion drawn by Yamakawa, that the mass transfer affects the heat transfer coefficient. Yamakawa, et al. (Reference 13) thought that the mass transfer could be eliminated by making the inlet humidity the same as that at the frost surface and to establish their conclusion, they took the convective heat as the only heat source at the frost surface. The heat flux, however, as measured at the wall below the frost layer, is greater than the convective heat because, due to the temperature gradient driving force, the latent heat is also being released in the frost layer. There is no evidence that any correction was made for the latent heat contribution and thus, an incorrect interpretation of the data was obtained. Yamakawa (Reference 13), also makes the point that the water vapor nucleates in the thermal boundary layer above the frost surface. This process releases the latent heat and causes a change in the temperature profile in the thermal boundary layer, as observed by Yamakawa, which would change the way the heat transfer coefficient is related to the Reynolds' number. However, in the turbulent forced convection limit, (i.e.,  $Re \geq 10^4$ ) the heat and mass transfer mechanisms are effectively decoupled because the sensible heat flux is much greater than the heat flux generated by the release of the latent heat through freezing. Therefore, it can be assumed that the latent heat release rate has a negligible effect on the heat transfer coefficient.

On the other hand the heat transfer coefficient is affected by the frost surface roughness. From our analysis of Yamakawa, et al. data (Reference 13), the ratio of the effective area of the frost surface to a smooth area is found to be a constant at 1.95. The frost roughness variety has no effect on  $h_H$  because the boundary layer is already turbulent and  $h_H$  is experimentally independent of the frost porosity. Therefore, the usual heat transfer coefficient is increased by a factor,  $r = 1.95$ , as is shown by the correlation,

$$Nu = \frac{h_H D_e}{k_a} = 0.021 Re^{.8} Pr^{.6} \text{ with } h_H^* = h_H(1.95), \quad (62)$$

where  $h_H$  = heat transfer coefficient of empirical equation and  $h_H^*$  = experimental heat transfer coefficient.

Equation (62) is believed to be the most accurate to date for calculating the heat transfer coefficient over frost and is being used as the correlation for turbulent forced convection. There is very little scatter when applying Equation (62) to Yamakawa's data, (Reference 13) even for points corresponding to relative humidities from 56% to 97% as shown in Figure 9. Furthermore, the points corresponding to the different humidities show no preferred bias. This supports the assumption that the nucleation in the boundary layer has a negligible effect on the heat transfer coefficient in this experimental data.

The mass transfer coefficient could be obtained from heat transfer coefficient using the Chilton - Colburn analogy (Reference 6). However, Yamakawa's data (Reference 13) shows a strong scatter for the analogy of the heat and mass transfer. It is difficult to determine what causes the scatter of the  $h_H^*$  vs  $h_m^*$  (experimental mass transfer coefficient) plot shown in Figure 10, because the points are not identified by the corresponding humidities and Reynolds number, yet certain trends can be perceived. For a mass transfer coefficient less than about 30  $g/m^2s$ , where  $h_m = h_m^*$ ,  $h_m^*$  can be calculated as if from the Chilton - Colburn analogy shown as the upper line in Figure 10,

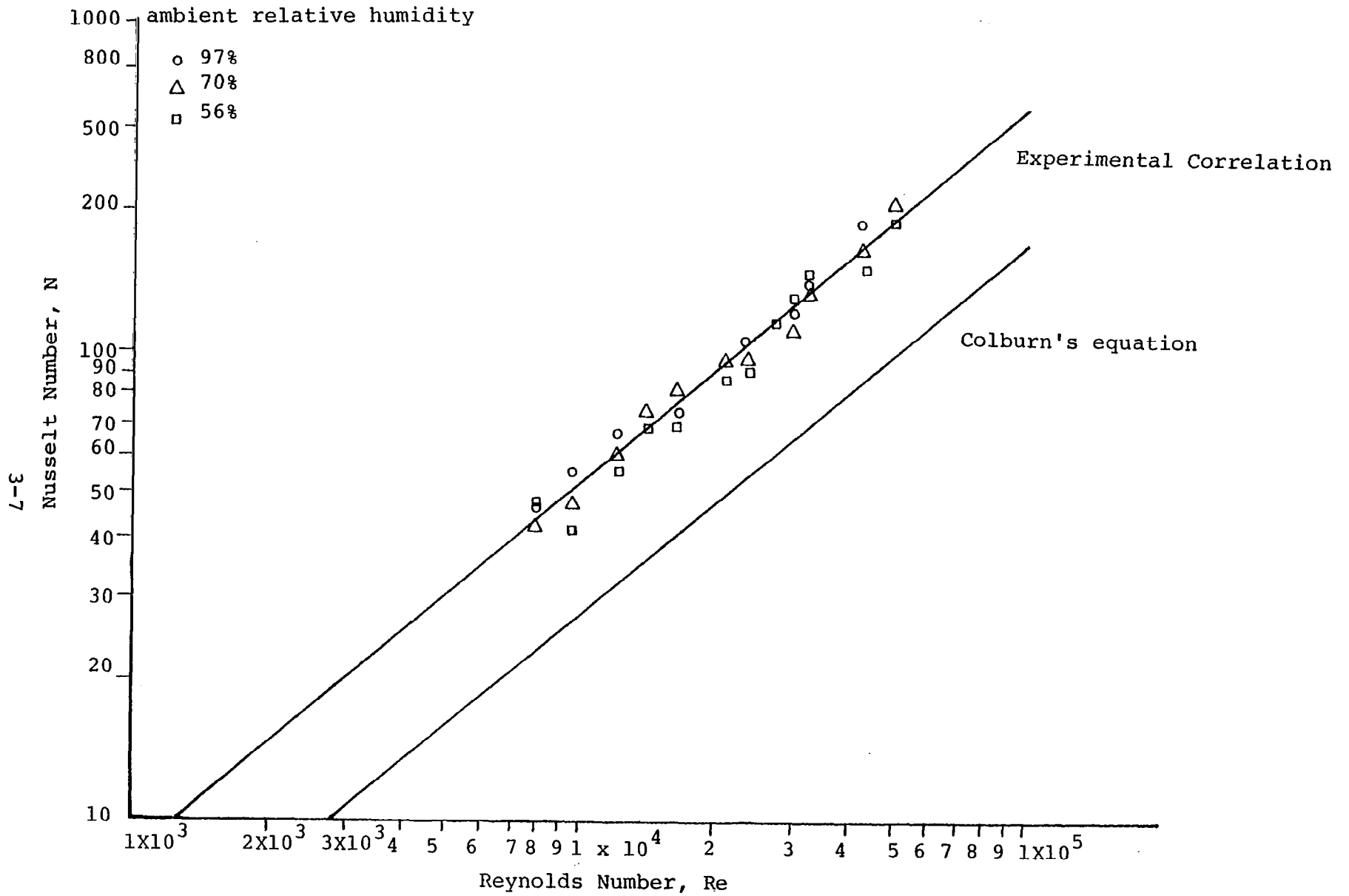


Figure 9. Relationship between Nusselt's number and Reynolds' number (Reference 13)

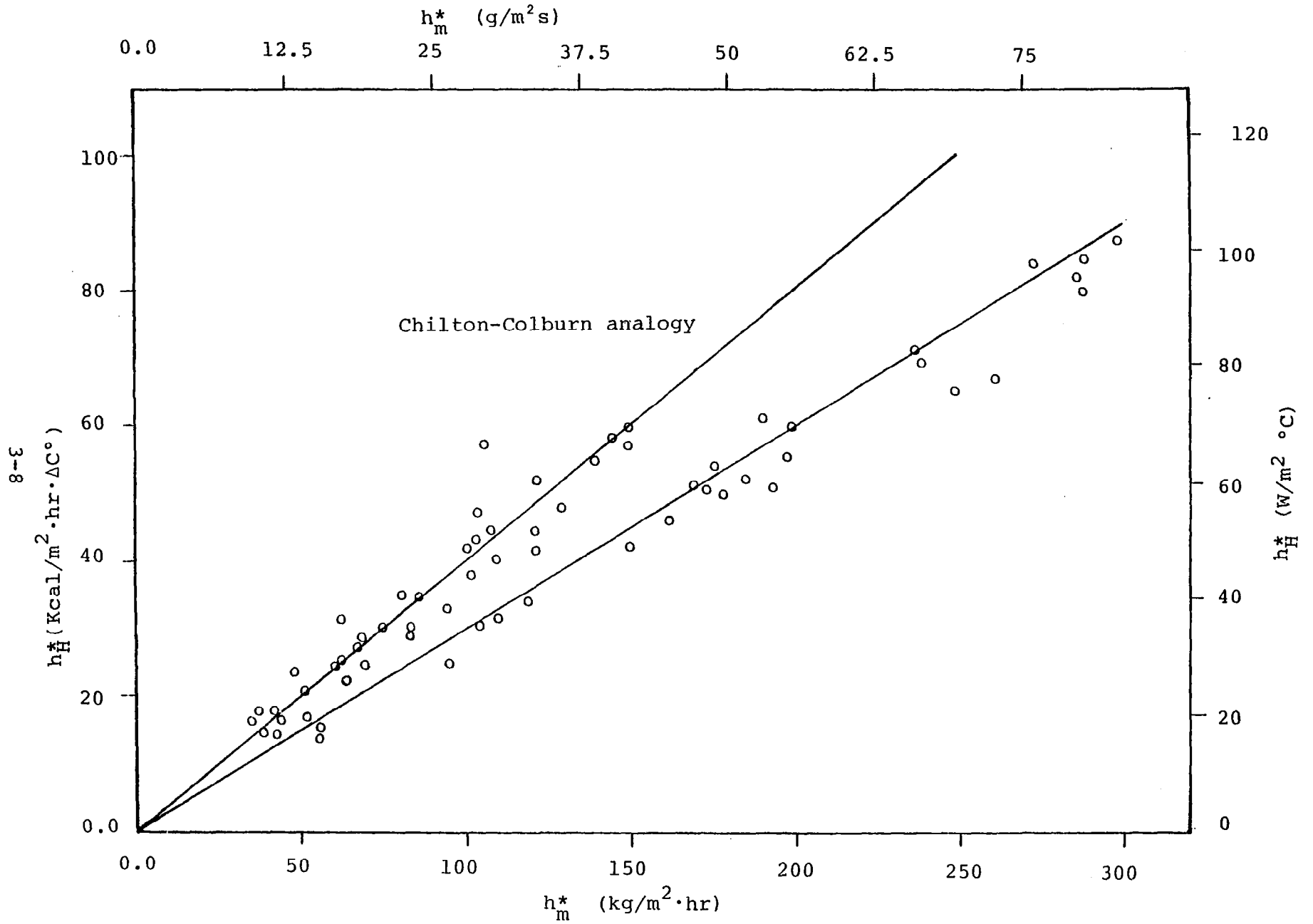


Figure 10. Relationship between local heat and mass transfer coefficient (Reference 13)

$$\frac{h_H^*/1.95}{h_m^*} = h_H/h_m^* = C_p Le^{-2/3} \quad (63)$$

This correlation seems to rule out the effect of the surface roughness on the experimental mass transfer coefficient,  $h_m^*$ . But this correlation is tentative because in the turbulent flow the mass transfer coefficient should be affected by the surface roughness in the same way as the heat transfer coefficient is.

At  $h_m^* = 30 \text{ g/m}^2\text{s}$  one can see a very strong scatter in the data, and it is biased in such a way that one can propose a mass flux enhancement due to nucleation in the thermal boundary layer. By using Epstein and Rosner's approach (Reference 11), it can be shown that for the wide range of wall temperatures and ambient humidities, the water vapor mass flux increases by a factor from 1.0 to a maximum of 2.95 over the usual mass flux of condensation on the wall surface. That is,

$$1 \leq h_m^*/h_m \leq 2.95 \quad (64)$$

For the mass transfer coefficient greater than  $45 \text{ g/m}^2\text{s}$ , the Chilton - Colburn analogy between  $h_H^*$  and  $h_m^*$  can be modified to

$$h_H^*/h_m^* = 1.5 C_p Le^{-2/3} \quad (65)$$

shown as the lower line in Figure 10, which means that the enhancement factor is  $h_m^*/h_m = 1.3$ . That is, if the Chilton - Colburn analogy is still valid for a rough surface and a turbulent flow.

### 3.3 SUMMARY OF HEAT AND MASS TRANSFER COEFFICIENT EQUATIONS

So far we have considered the extremes of the experimental data. At one extreme we have the laminar natural convection, and at the other extreme we have the turbulent forced convection. In the region of combined natural and forced convection not only the heat and mass transfer are coupled but also the nucleation in

the boundary layer and the frost surface area affect the heat transfer to a significant degree. The surface roughness will affect the heat transfer in two ways. The first is that the surface roughness will cause the transition point (located between laminar and turbulent zones) to occur closer to the leading edge. Secondly, in the laminar zone, the effective surface area for the heat transfer coefficient is unity relative to the smooth surface area, but the effective area is 1.95 times greater than the smooth surface area in the fully turbulent zone. Although the effects of nucleation in the thermal boundary layer upon the heat transfer was considered negligible in both extreme experimental data, it may become significant in the combined natural and forced convection when the latent heat release rate in the boundary layer may become the same order of magnitude as the sensible heat. Lastly, from our studies of the data, the perturbations in the mass transfer coefficients is caused by the fog formation or nucleation in the boundary layer and by the frost surface roughness. The maximum enhancement in the mass transfer coefficient appears to be at the ratio,  $h_m^*/h_m = 1.3$ .

For the comparison of the frost formation model to experimental data, Equations (55) to (60), (62) and (65) will be used tentatively. The frost formation model however, can be immediately generalized to other air flow geometry, and surface roughness conditions, if the heat and mass transfer coefficients can be obtained for these conditions. To obtain the transfer coefficients for an arbitrary airfoil geometry, computer programs need to be developed to couple the boundary layer models with the potential flow models. There are such programs in the literature (References 18, and 19) but none has yet satisfied our requirements to include the effect of water vapor mass flux nucleation and surface roughness on the flow properties near the wall. Some literature (References 20, and 21) provides ways of calculating the influence of surface roughness and the water vapor mass flux on the transfer coefficients. Other literature (References 22 and 23) provide ways of calculating the enhancement of the

mass transfer coefficient due to nucleation in the boundary layer. Only a small amount of literature is available for analyzing the heat and mass transfer problem for combined natural and forced convection. A synthesis of this literature will be required for the study of overnight frost formation on an aircraft.

SECTION 4  
THE SIMULATION OF FROST FORMATION

4.1 FROST FORMATION MODEL

In Section 2, the frost thermal conductivity was formulated so that the heat flux through the frost layer could be calculated. In Section 3, the heat and mass transfer coefficients were formulated so that the heat flux to the frost surface from the air could be calculated. By matching the two heat fluxes at the frost surface the temperature of the frost surface can be calculated. The frost surface temperature will change with time because the frost layer is becoming denser and thicker, which in turn affects the computations of the heat flux in the frost layer. During the process of frost formation it is assumed that the part of the water vapor transported to the surface freezes at the surface so as to increase the thickness of the frost. The remaining water vapor is diffused into the existing frost layer before it freezes. Since the frost density is assumed to be spatially invariant in a direction normal to the plate, the water vapor diffusion flux entering the frost surface from the surrounding air is given by

$$\dot{m}_{ds} = \frac{\partial \rho_f}{\partial t} x_s \quad , \quad (66)$$

where  $\dot{m}_{ds}$ ,  $\rho_f$  and  $x_s$  stand for water vapor diffusion mass flux at the surface, frost density and frost thickness respectively. Also, the water vapor mass flux,  $\dot{m}_d$  will obey the diffusion Equation (18) and will be driven by the temperature gradient throughout the frost layer.

The water diffusion flux is given by Equation (22)

$$\dot{m}_d = \frac{D\beta}{(1-\chi)\tau_s} \left( \frac{P_v}{R_v T^2} \right) \left( \frac{L_s}{R_v T} - 1 \right) \frac{dT}{dx} \quad . \quad (67)$$

Equation (67) can be evaluated at the frost surface if the frost surface temperature  $T_s$ , the temperature gradient  $\left. \frac{dT}{dx} \right|_s$ ,

and the frost thickness  $x_s$  are known. Combining Equations (66) and (67) allows the frost density to be solved for as a function of time.

To obtain a value for frost surface temperature,  $T_s$ , the quasi-steady-state heat equation for the frost layer is to be solved. This is, the equation

$$K \frac{dT}{dx} = q_o \quad (68)$$

with  $K$  given by Equation (42) is to be solved with the boundary conditions

$$T = T_s \text{ at } x = x_s \quad \text{and} \quad T = T_w \text{ at } x = 0,$$

where

$$q_o = h_H (T_a - T_s) + h_m L_s (\rho_a - \rho_{vs}) / \rho_a + \epsilon \sigma (T_a^4 - T_s^4). \quad (69)$$

This gives

$$\int_{T_w}^{T_s} K dT = x_s q_o. \quad (70)$$

The temperature gradient at the frost surface is given by

$$\left. \frac{dT}{dx} \right|_s = \frac{q_o}{K(T_s)}. \quad (71)$$

The thickness of the frost can be computed from the weight of the frost ( $\rho_f x_s$ ) which is directly related to the mass transfer coefficient and the water vapor density by

$$\begin{aligned} \frac{d(\rho_f x_s)}{dt} &= h_m (\rho_a - \rho_{vs}) / \rho_a \\ &= h_m (\omega_a - \omega_s), \end{aligned} \quad (72)$$

Since these equations cannot be solved analytically, numerical techniques are used to solve these equations to obtain the thickness and the density of the frost.

## 4.2 THE NUMERICAL SCHEME FOR FROST FORMATION MODEL

The scheme begins by assuming a small initial value of frost density,  $\rho_{f0}$  and frost thickness,  $x_{s0}$ . The initial frost density is set equal to that of the ambient air, i.e.,  $\rho_{f0} = \rho_a(1 + \omega_a)$  and the initial thickness is calculated by

$$x_{s0} = h_m^* (\omega_a - \omega_w) (\Delta t_0) / \rho_{f0} \quad , \quad (73)$$

where  $\omega_w$  is the absolute humidity at wall temperature and  $\Delta t_0$  is set at one second. The frost surface temperature,  $T_s$  is obtained from the monotonic nonlinear equation,

$$\int_{T_w}^{T_s} K dT = x_s \left[ h_H(T_a - T_s) + h_m L_s (\omega_a - \omega_s) + \epsilon \sigma (T_a^4 - T_s^4) \right] \quad (74)$$

In order to solve this equation in an accurate and efficient manner, the frost thermal conductivity given by Equation (42) is first interpolated by a parabolic function in a temperature range  $\Delta T$  and integrated to get the first term in Equation (74), (i.e.,  $\Delta T$  is often greater than  $T_s - T_w$ ). Then  $T_s$  in Equation (74) is solved for by an interval-halving-iterative technique so that the left term of Equation (74) is equal to the right terms. In this way successive evaluations of the complicated thermal conductivity expression (i.e., Equation (42)) and numerical integrations can be completely avoided when iterating to get  $T_s$ . The temperature gradient at the frost surface is obtained by

$$\left. \frac{dT}{dx} \right|_s = \frac{\int_{T_w}^{T_s} K dT}{K(T_s) x_s} \quad . \quad (75)$$

The value for the frost density is predicted for a later time  $t_{n+1}$  by using the equation,

$$\frac{\partial \rho_f}{\partial t} = \frac{DB}{(1-X) \tau_s x_s} \left( \frac{P_{vs}}{R_v T_s^2} \right) \left( \frac{L_s}{R_v T_s} - 1 \frac{dT}{dx} \right) \Big|_s \quad , \quad (76)$$

which is solved by using a second order Runge Kutta "initial" scheme, and by a second order predictor-corrector "takeover" scheme. Finally, the value for the frost thickness is predicted for the same time as the frost density, (i.e., at  $t_{n+1}$ ) by the equation,

$$\rho_f x_s = \int_{t_0}^{t_{n+1}} h_m (\omega_a - \omega_s) dt + \rho_{f0} x_{s0} , \quad (77)$$

where the rectangular rule is used for the integration, in acknowledgement of the fact that  $h_m$  and  $\omega_s$  are slowly changing functions of time. At the same particular time,  $t_{n+1}$ , a new frost surface temperature is calculated by returning back to Equation (74) incrementing  $n$ , and using the new values of frost density  $\rho_f$  and thickness  $x_s$ .

## SECTION 5

### COMPARISON OF THE MODEL WITH THE AVAILABLE EXPERIMENTAL DATA

In this section, three separate classes of experimental data which are considered to be complete and the transfer coefficients considered to be well known are described and compared with results predicted by the frost formation model.

The first set of experimental data that the model predicts quite accurately is that of Brian, et al. (Reference 1). Since the typical Reynolds number is greater than 10,000 and the boundary layer is turbulent in the duct in which their experiment was conducted, the correlation for the forced convection mentioned earlier by Equations (62) and (65) for the heat and mass transfer coefficients is used here. The roughness factor,  $r$ , is set at 1.95 and the enhancement factor is set at 1.3. It may be noted that these coefficients are based on the experimental data of Yamakawa, et al. (Reference 13). Table II lists the input data from Brian et al. (Reference 1) for the frost formation model and also the symbols identifying the experimental data in the next three figures.

Results from the model have been compared with the experimental data giving the frost weight, density, and thickness as functions of time under different experimental conditions. The results are given in Figures 11, 12 and 13 where the computer generated solid curves are plotted along with the experimental data. The figures show excellent agreement.

When the standard correlations given by Equations (49) and (52) instead of the modified Equations (62) and (65) are used in this set of data, the corresponding results are shown by the dashed curves. The comparison of the solid and the dashed curves based on the same experimental data shows that poor correlations are obtained for standard heat and mass transfer coefficients.

The second set of experimental data examined is that of Yamakawa et al. (Reference 13) for forced convection in a duct.

TABLE II

Data Input to the Frost Formation Model for Comparison  
With Brian et al. Data for Forced Convection (Reference 1)

Computer Curve No.	Experimental Graph Symbol	Reynolds Number	Relative Humidity (%)	Wall Temperature (°K)	Air Temperature (°K)
1	○	14500	26.1	79.83	297
2	△	9316	26.2	79.83	297
3	□	5603	26.0	79.83	297
4	●	14750	20.8	79.83	297
5	▲	9247	15.8	79.83	297
6	■	5625	16.2	79.83	297

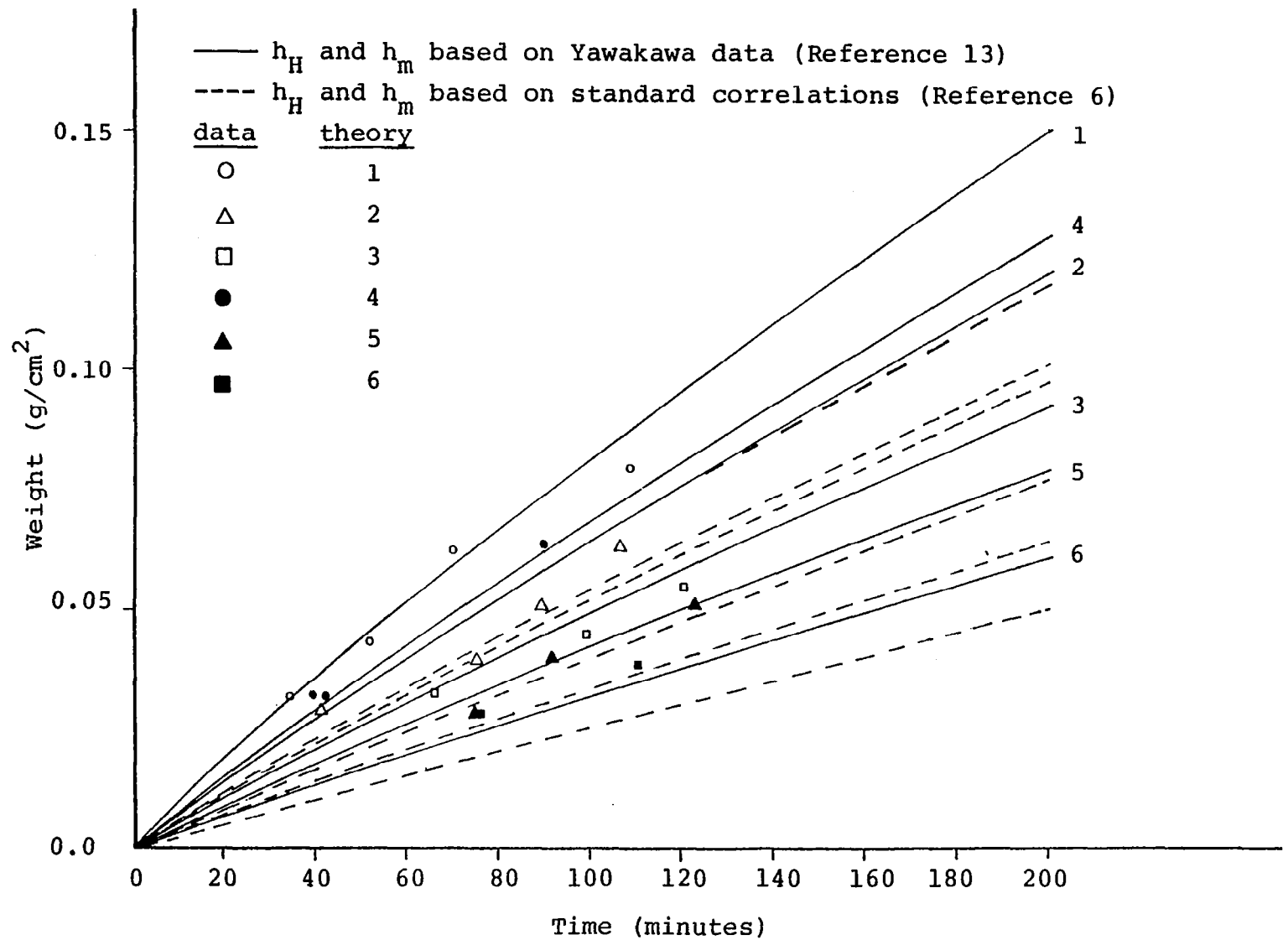


Figure 11. Weight versus Time for Brian et al. Data (Reference 1)

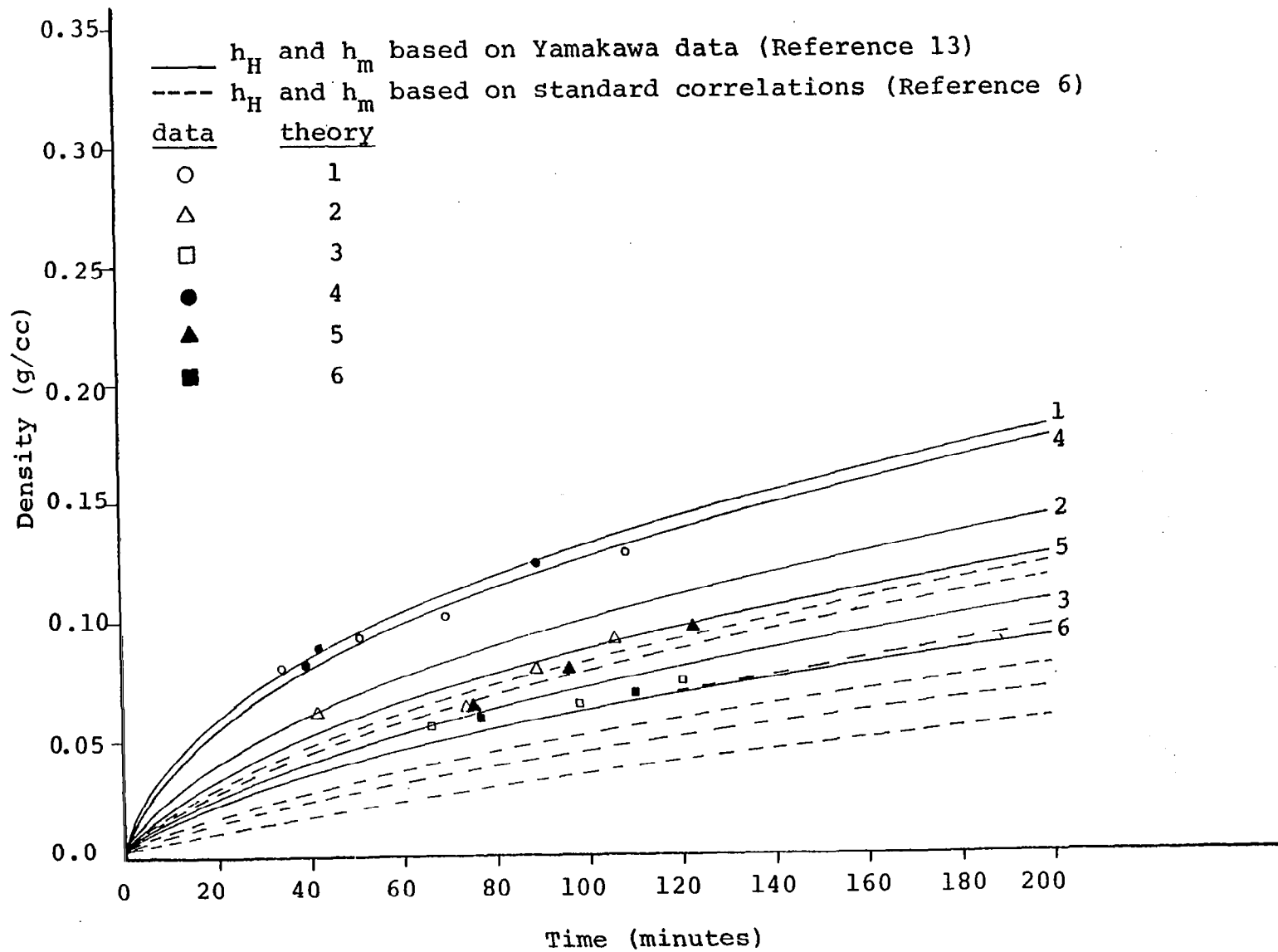


Figure 12. Density versus time for Brian et al. Data (Reference 1)

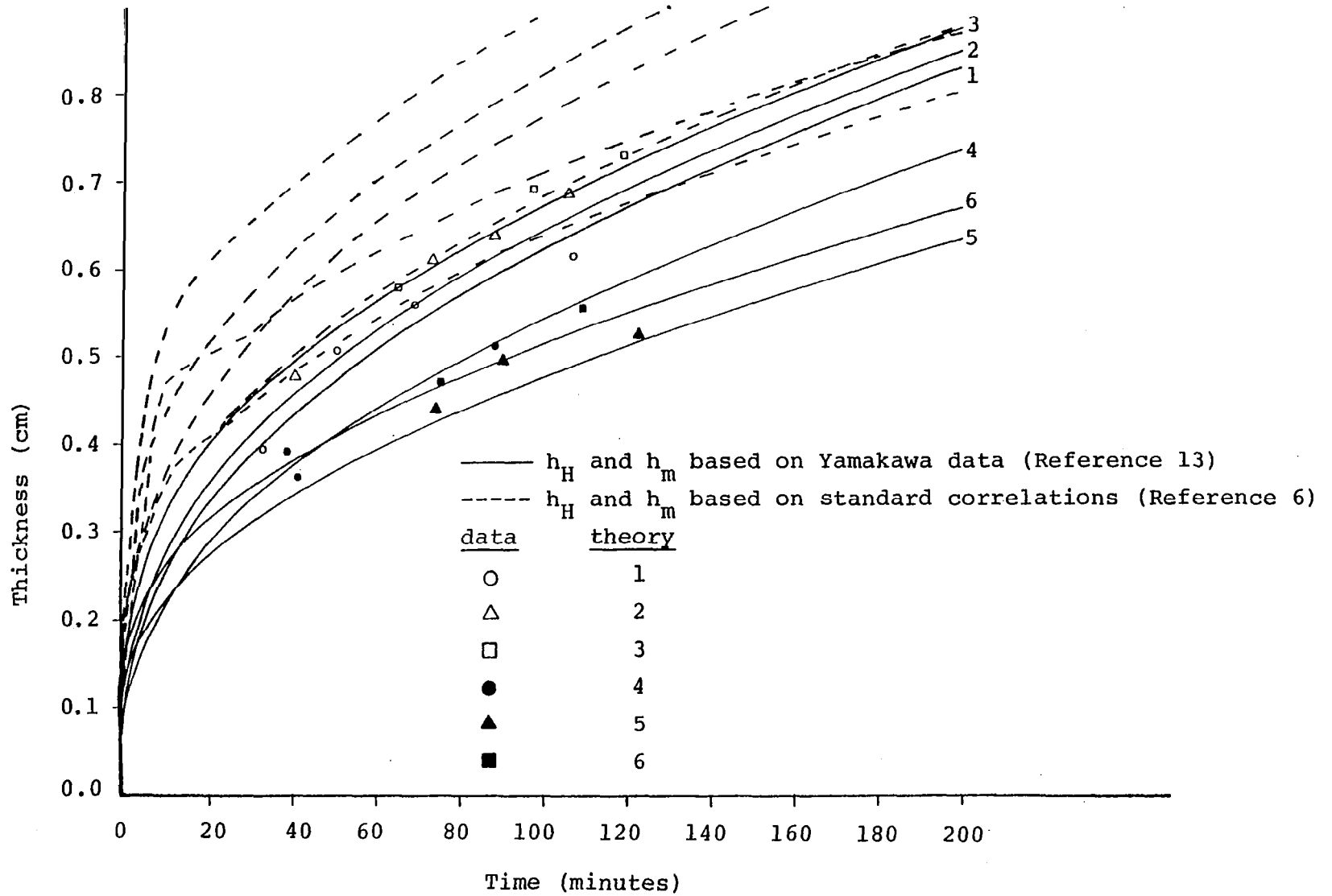


Figure 13. Thickness versus Time for Brian et al. Data (Reference 1)

The roughness factor and the enhancement factor are again set at 1.95 and 1.3 respectively.

Table III provides the input data into the frost formation model and Figures 14, 15 and 16 show the results of the computer generated solid curves along with the experimental data of frost weight, density, and thickness as functions of time. The dashed lines, generated using the standard correlations again, provide inferior results compared to the modified correlations.

Curves 1 to 4, in Figures 14 to 16, show a fair agreement with the experimental data. However, curve 5 shows a sharp disagreement with the data. The disagreement is probably due to the following complications. Since the relative humidity for this run is nearly 100%, the fog starts forming before the water vapor enters into the boundary layer. This means that the enhancement factor becomes unity. Secondly, the water droplets reaching the surface are large, which in turn cause the frost structure to consist of a relatively large number of spherical ice-droplets. This alteration in the frost structure lowers the thermal conductivity to under the computed value. Third, the frost surface temperature quickly reaches the melting temperature, which causes the frost thickness to stabilize and the frost density to increase over their modeled values. The possibility of modifying the present model to accommodate these three factors will be considered for future work.

The third set of experimental data examined is that of Nakamura, et al. (Reference 14) for natural convection on a vertical plate. The heat and mass transfer coefficients are given by Equations (55) and (56), and the thermal conductivity is the same as that used for the Yamakawa data (Reference 13). Table IV provides the input data into the frost formation model and Figures 17, 18 and 19 show the results of the computer generated curves along with the experimental data of frost weight, density, and thickness. Experimental data in the 5th and 6th entries of Table IV are not available for Figures 17 and 18.

TABLE III

Data Input to the Frost Formation Model for Comparison With Yamakawa, et al. Data for Forced Convection in a Duct (Reference 13)

Computer Curve No.	Experimental Graph Symbol	Air Velocity (m/s)	Relative Humidity (%)	Wall Temperature (°K)	Air Temperature (°K)
1	□	1.6	56.2	251	284
2	△	5.0	56.2	251	284
3	○	5.0	70.0	251	284
4	▲	7.3	56.2	251	284
5	●	7.3	97.4	251	284

Note: To calculate Reynolds Number, the hydraulic diameter is taken as  $D_e = 20(1.7-x_s)/(11.7-x_s)$  cm.

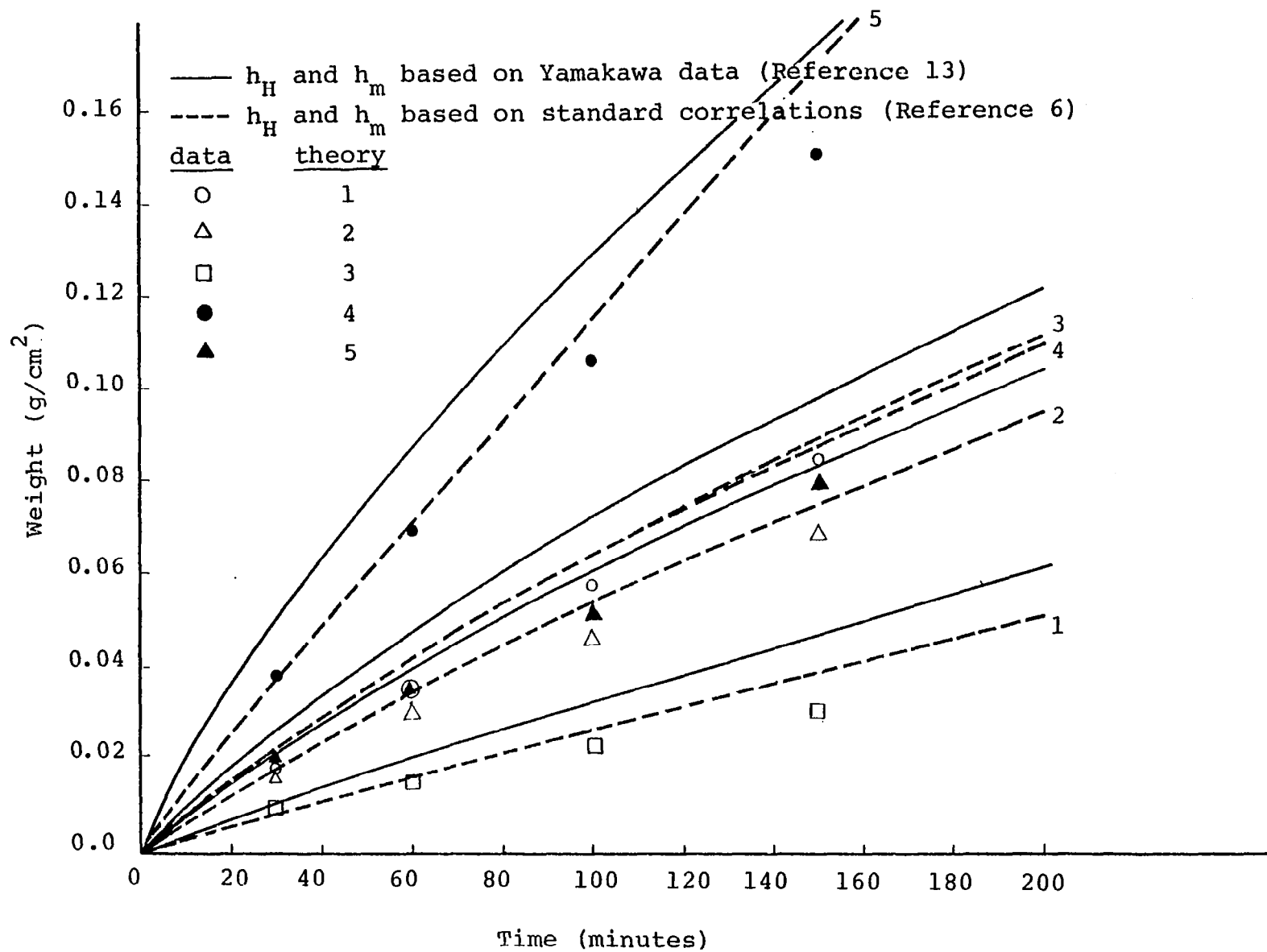


Figure 14. Weight versus Time for Yamakawa, et al. Data (Reference 13)

6-5

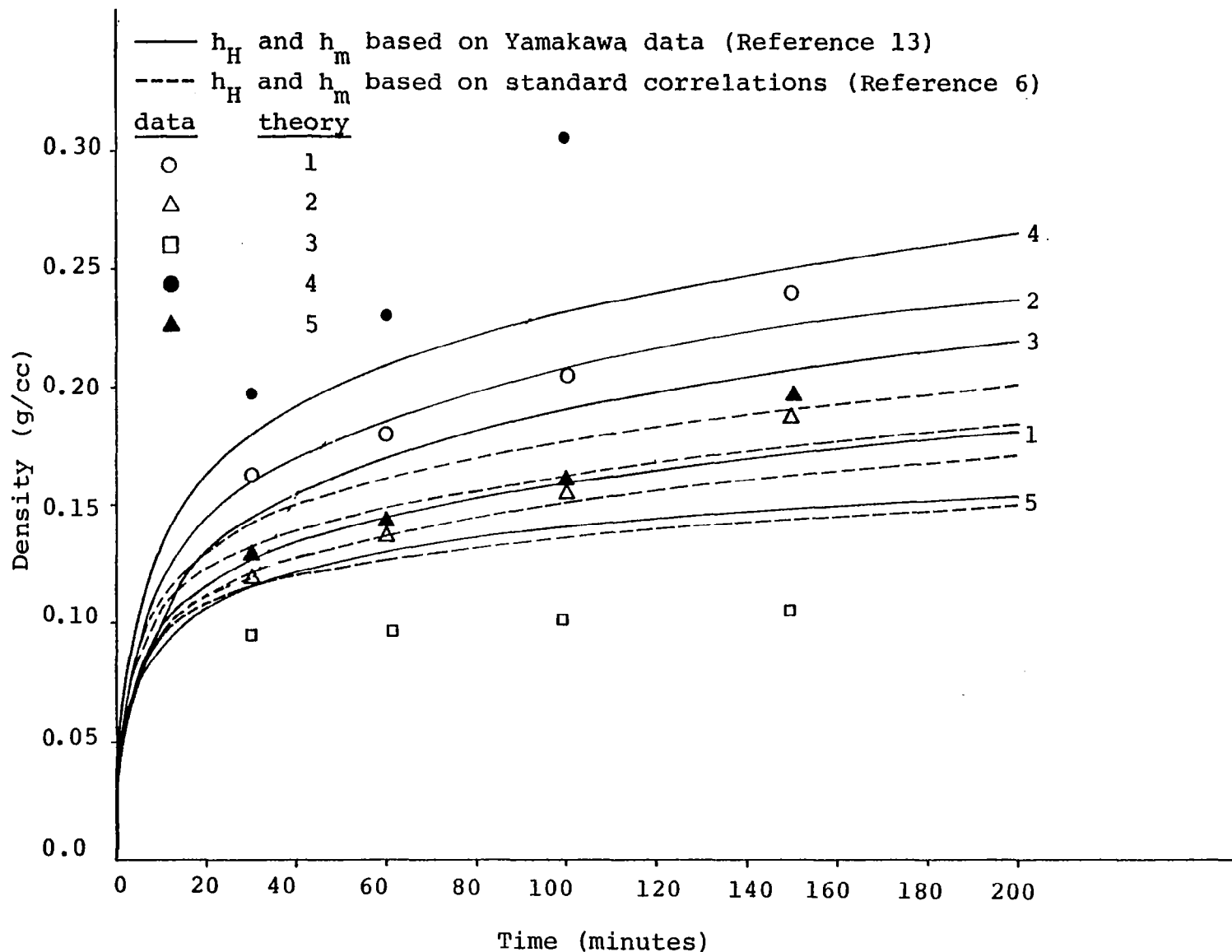


Figure 15. Density versus Time for Yamakawa, et al. Data (Reference 13)

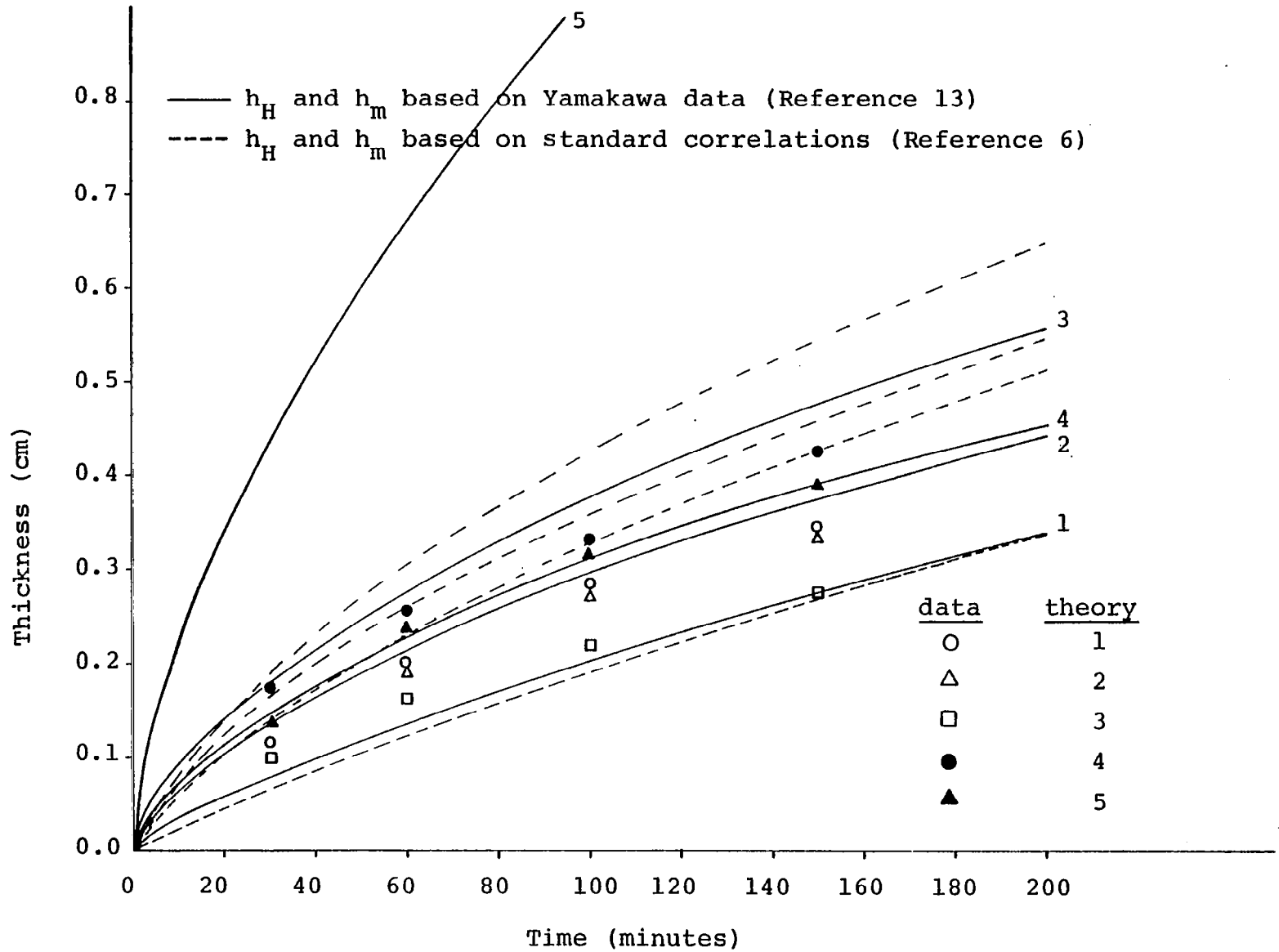


Figure 16. Thickness versus Time for Yamakawa, et al. Data (Reference 13)

TABLE IV

Data Input to the Frost Formation Model for Comparison With Nakamura  
Data for Natural Convection on Vertical Plate (Reference 14)

Computer Curve No.	Experimental Graph Symbol	Plate Height (meters)	Ambient Relative Humidity (%)	Wall Temperature (°K)	Air Temperature (°K)
1	○	0.085	74	262.46	301.06
2	△	0.085	76	259.66	296.36
3	□	0.085	75	257.36	292.56
4	●	0.085	61	260.76	286.36
5	▲	0.040	53	256.56	291.96
6	■	0.040	38	258.76	291.66

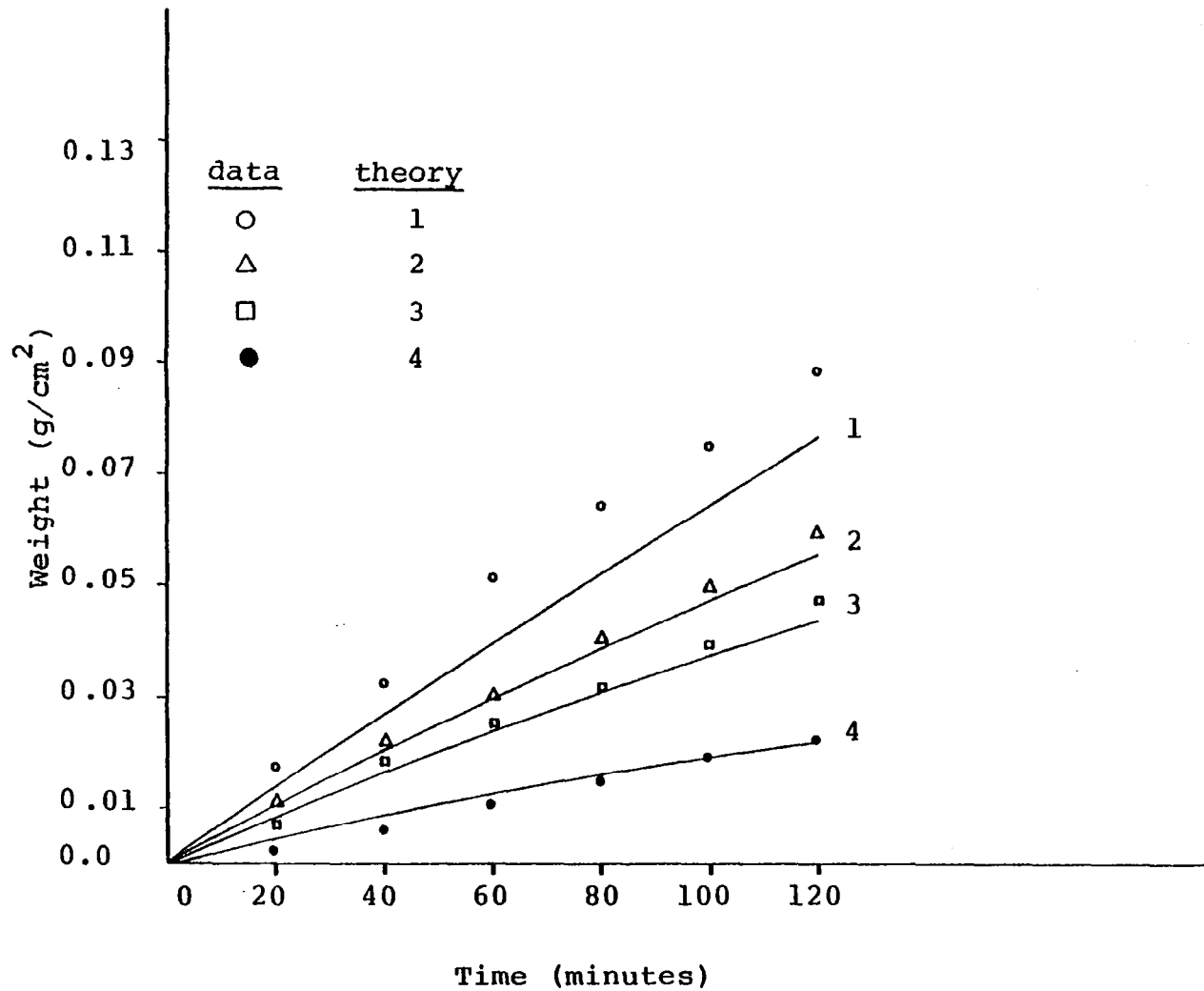


Figure 17. Weight versus Time for Nakamura Data (Reference 14)

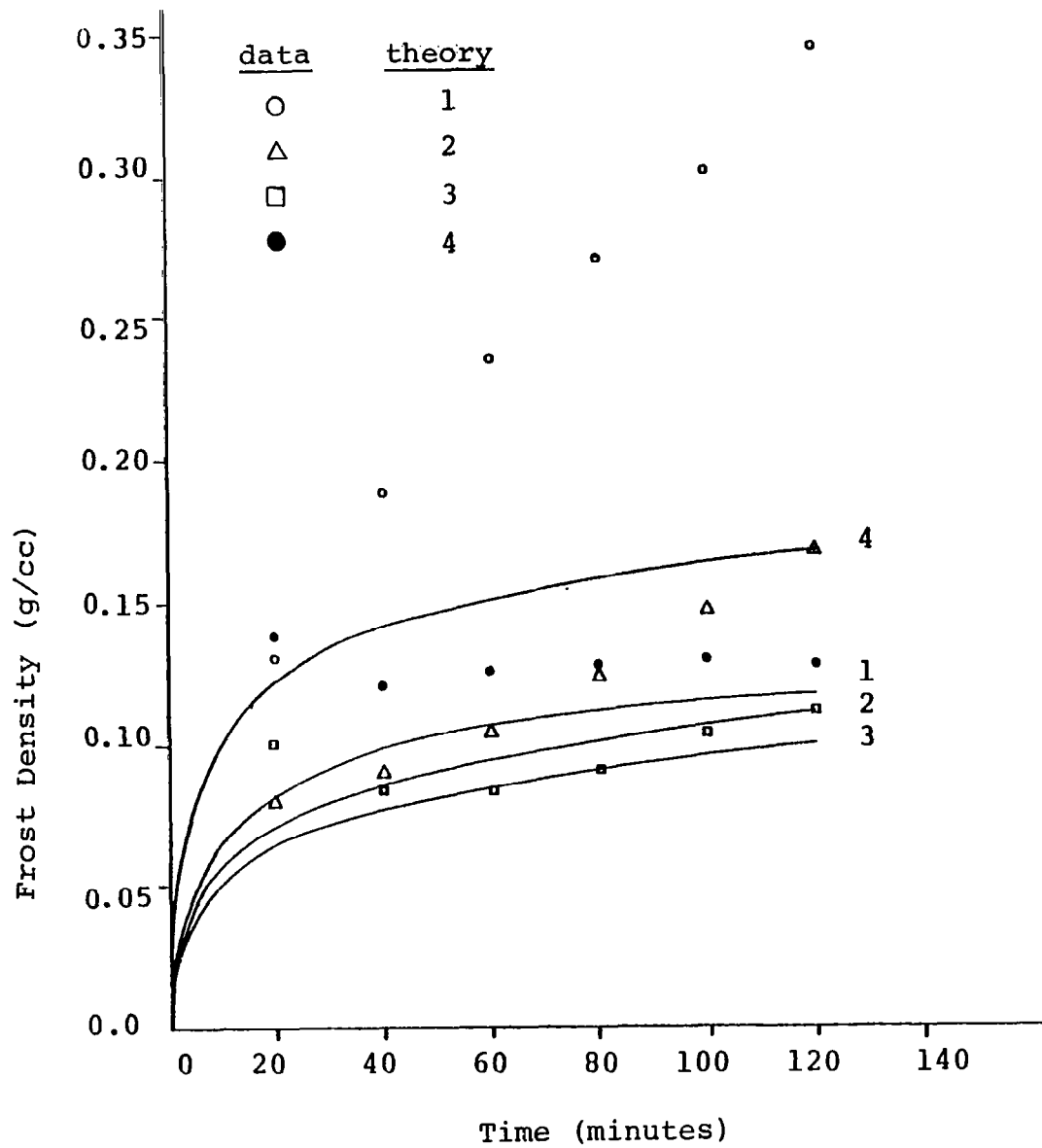


Figure 18. Density versus Time for Nakamura Data (Reference 14)

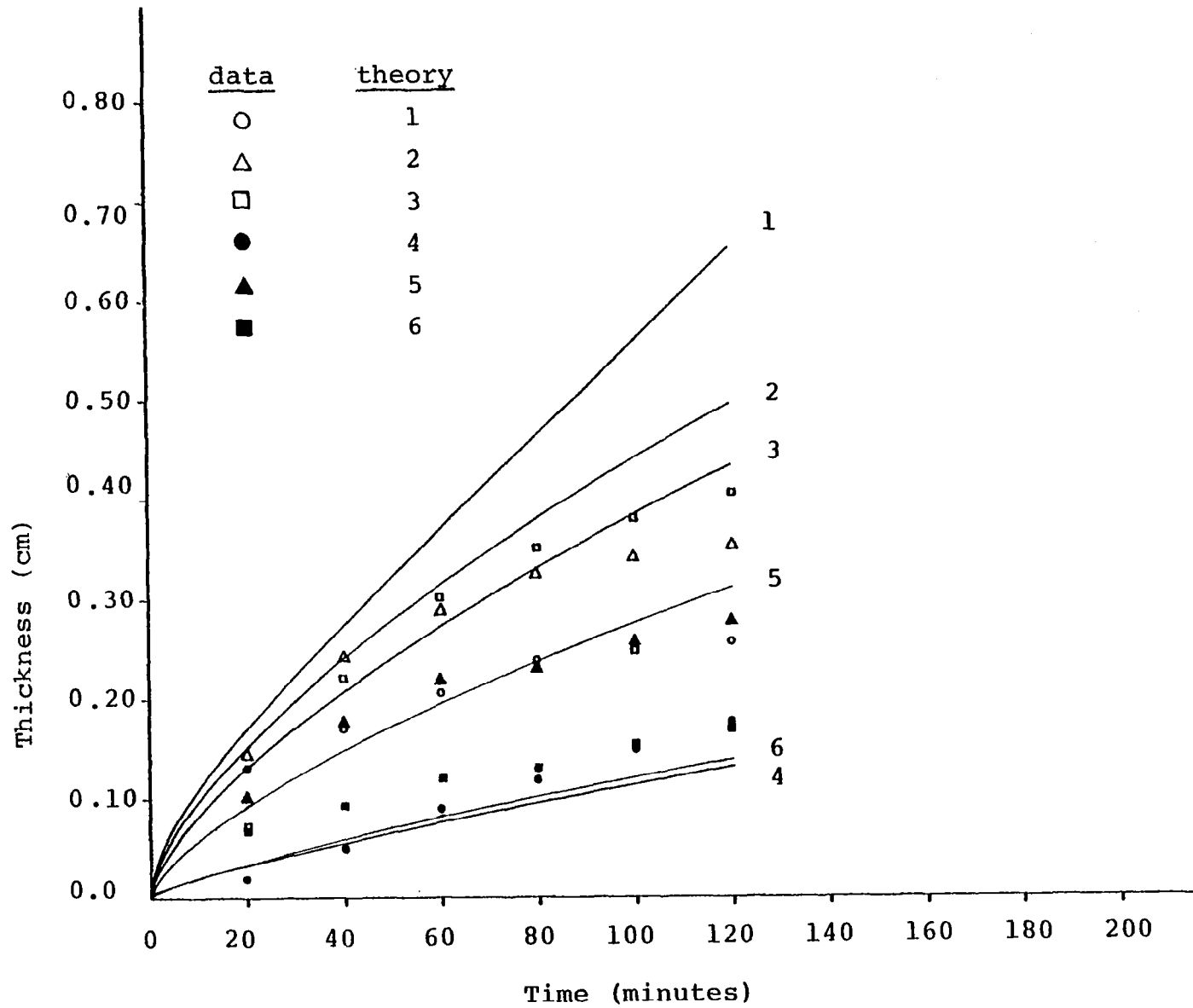


Figure 19. Thickness versus Time for Nakamura Data (Reference 14)

It is interesting to note that the curves 2, 3 and 4 in Figure 17 show a very good agreement with the experimental data. This verifies the accuracy of the mass transfer coefficient calculated in this experiment. However, the curves 1 and 2 in Figure 18 show a disagreement with the experimental data of frost density and thickness versus time. The main reason seems to be that the frost surface starts melting very early, causing the thickness to stabilize sooner and the frost density to increase over its modeled value.

SECTION 6  
SUMMARY AND RECOMMENDATIONS

Keeping in view the complexity of the problem and the sparse experimental data available, the results obtained to date are very encouraging. The good agreement of the proposed model with the three sets of experimental data available has encouraged us to further develop this model for use in evaluating the aerodynamic penalties on an aircraft having frost on its wings. Although the equations used in the present model for calculating the frost density as a function of time has done remarkably well for most frost formations, new equations must be developed to calculate the change in frost density due to liquid water seepage into the frost and for a non-spatially-uniform frost density. To realistically apply the frost formation model to an airfoil, additional considerations must also be given to the enthalpy rate terms for the aircraft skin and the frost, the complex black-body radiation to space, and the transfer coefficients for the various flow regimes and airfoil geometries. The formulation of the frost thermal conductivity used in the model has been placed on more theoretical grounds than in any previous approaches. As a consequence, the empiricism has been reduced to determining a structure parameter,  $\beta_c$ , tentatively given by Equation 48, which covers nearly all the experimental data examined to date. However, the validity of the structure parameter  $\beta_c$  needs to be verified at high frost density for the various values of wall-temperature.

In summarizing, the present model for frost formation was constructed with a view towards its application to the overnight frost formation on an airfoil. The model contains many complexities not considered by any previous investigator. To obtain an improvement in the present model of frost formation would require more complete experimental data. In particular, specific experiments should be performed to improve our knowledge of the heat and mass transfer coefficients, improve the frost density

It is recommended that further development of the present frost model for utilization in the Aircraft Takeoff Simulation Program proceed along the following lines. Additional terms should be added to the heat balance equations to allow for radiation heat loss of the skin of the airfoil to space. This is the mechanism in nature that produces the rapid cooling of the airfoil, relative to the surrounding air, and results in frost formation. The resulting model could then be evaluated by comparison of computer results with experimental data. The experimental data, consisting of frost density and thickness values, would be obtained from measurements on a flat plate exposed to the environment during atmospheric conditions conducive to frost formation. Monitoring of the atmosphere during the frost formation period would provide the input data to test the computer model versus the actual observational data. The predictive capabilities of the model could also be tested. Using meteorological predications of the overnight temperature, pressure and cloud cover profiles, the computer model would be run to determine the anticipated frost accumulation by morning. This result would then be compared with the actual accumulation to assess the frost prediction capabilities of the model. An accurate frost prediction model giving reliable estimates of frost thickness and density would provide significant benefits to the aviation community.

Finally after having established the validity of the frost model it should be incorporated into an aircraft simulation program to assess aerodynamic penalties during takeoff. In addition to providing the initial frost condition at takeoff, the model would be used throughout the takeoff phase of operation to determine the frost dissipation, or further accumulation, on the airfoil as the speed of the aircraft increases.

rate modeling, especially with respect to water seepage, and obtain a more refined empirical formulation of the structure parameter,  $\beta_c$ .

## SECTION 7

### REFERENCES

1. Brian, P.L.T., Reid, R.C. and Brazinsky, I., "Cryogenic Frost Properties", Cryogenic Technology, Sept./Oct. 1969.
2. Shah Y. T., Sc.D Thesis M.I.T. 1968.
3. Biguria and Wenzel "Measurement and Correlation of Water Frost Thermal Conductivity and Density", Vol. 9 No. 1, I & EC Fundamentals, February 1970, p. 129.
4. White, J., "Heat and Mass Transfer in Thick Frost Layers", Ph.D. dissertation University of Kentucky, Mechanical Engineering Department, 1973.
5. Jones, B.W. and Parker, J.D., "Frost Formation with Varying Environmental Parameters", Trans. ASM Journal of Heat Transfer, May 1975.
6. Rohsenow, W.M. and Hartnett, J.P., "Handbook of Heat Transfer", McGraw-Hill Book Company, 1973.
7. White, J. and Cremers, C.J., "Prediction of Growth Parameters of Frost Deposits in Forced Convection", AIAA/ASME 1974 Thermophysics and Heat Transfer Conference, Boston, Mass., July 15-17, 1974.
8. Dillard, D.S. and Timmerhaus, K.D., "Low Temperature Thermal Conductivity of Selected Dielectric Crystalline Solids", Thermal Conductivity Proceedings of the Eighth Conference, Eds C.T. Ho and R.E. Taylor, Plenum Press. New York, p. 949, (1969).
9. Laubitz, M.J., "Thermal Conductivity of Powders", Can. J. Phys. Vol. 37 (1959).
10. Brian, P.L.T., Reid, R.C. and Shah, Y.T., "Frost Deposition on Cold Surfaces", J. Engg. Chem., Fundamentals Vol. 9, 1970.
11. Rosner, D.E. and Epstein, M., "Fog Formation Conditions Near Cool Surfaces", Journal of Colloid and Interface Science, Vol. 28, No. 1, September 1968.

12. New York American Society of Heating and Air Conditioning Engineering, "Heating, Ventilating, Air Conditioning Guide", Vol. 37, 1959 pp. 22-25.
13. Yamakawa, N., Takahashi, N. and Ohtani, S., "Forced Convection Heat and Mass Transfer Under Frost Conditions", Heat Transfer-Japanese Reserch, Vol 1, No. 2, 1972.
14. Nakamura, H. "Free Connective Heat Transfer From Humid Air to a Vertical Plate Under Frosting Conditions", Bull. J.S.M.E., Vol. 17, 1974.
15. Brazinsky, I., Sc.D Thesis M.I.T. 1967.
16. Kays, W.M. and Perkins, H.C., "Forced Convection Internal Flow in Ducts", section 7 page 33, Handbook of Heat Transfer, Eds W.M. Rohsenow and J.P. Hartnett, 1973.
17. Okino and Tajima, "Heat and Mass Transfer by Free Convection Under Frosting Conditions", Translated by Osamu Tajima, originally published in Reito, 48, p. 338-349, (1973).
18. Hess, J.L., "A Fully Automatic Combined Potential Flow/Boundary Layer Procedure for Calculating Viscous Effects on the Lifts and Pressure Distributions of Arbitrary Three-Dimensional Configurations", Naval Ship Research and Development Center, Bethesda, Maryland 20084, Report No. MDC-J7491, June 1, 1977.
19. Dvorak, F.A., Woodward, F.A. and Maskew, B., "A Three-Dimensional Viscous/Potential Flow Interaction Analysis Method for Multi-Element Wings", NASA Ames Research Center, Moffet Field, California 94035, NASA-CR-152012, July 1977.
20. Healzer, J.M., Moffat, R.J. and Kays, W.M., "The Turbulent Boundary Layer on a Porous Rough Plate: Experimental Heat Transfer with Uniform Blowing", AIAA Paper No. 74-680 and ASME Paper No. 74-HT-14, AIAA/ASME 1974 Thermophysics and Heat Transfer Conference, Boston, 15 July 1974.
21. Dirling, R.B., "A Method for Computing Roughwall Heat Transfer Rates on reentry Nosetips", AIAA Paper No. 73-763, AIAA 8th Thermophysics Conference, Palm Springs, Ca., 16 July 1973.

22. Epstein, M., "Nonequilibrium Fog Formation within the Thermal Boundary Layer", Ph.D. Dissertation, Polytechnic Inst. of Brooklyn, June 1969.
  
23. Sherwood, T.K., Pigford, R.L., Wilke, C.R., "Mass Transfer", McGraw-Hill, New York, 1975.

1. REPORT NO. NASA CR-3129	2. GOVERNMENT ACCESSION NO.	3. RECIPIENT'S CATALOG NO.	
4. TITLE AND SUBTITLE Frost Formation on an Airfoil: A Mathematical Model I		5. REPORT DATE April 1979	6. PERFORMING ORGANIZATION CODE
		8. PERFORMING ORGANIZATION REPORT # UDR-TR-78-123	
7. AUTHOR(S) Mark Dietenberger, Prem Kumar, and James Luers		10. WORK UNIT NO. M-283	11. CONTRACT OR GRANT NO. NAS8-31294
9. PERFORMING ORGANIZATION NAME AND ADDRESS University of Dayton Research Institute Dayton, Ohio 45469		13. TYPE OF REPORT & PERIOD COVERED Contractor (Final Report)	
		14. SPONSORING AGENCY CODE	
12. SPONSORING AGENCY NAME AND ADDRESS National Aeronautics and Space Administration Washington, D. C. 20546			
15. SUPPLEMENTARY NOTES Prepared under the technical monitorship of the Atmospheric Sciences Division, Space Sciences Laboratory, NASA Marshall Space Flight Center, Alabama			
16. ABSTRACT A computer model to predict the frost formation process on a flat plate was developed for application to most environmental conditions under which frost occurs. The model was analytically based on a generalized frost thermal conductivity expression, on frost density and thickness rate equations, and on modified heat and mass transfer coefficients designed to fit the available experimental data. The broad experimental ranges reflected by the extremes in ambient humidities, wall temperatures, and convective flow properties in the various publications which were examined served to severely test the flexibility of the model. An efficient numerical integration scheme was developed to solve for the frost surface temperature, density, and thickness under the changing environmental conditions. The comparison of the results with experimental data was very encouraging.			
17. KEY WORDS Frost Ice Aircraft icing Aviation safety		18. DISTRIBUTION STATEMENT Category 47	
19. SECURITY CLASSIF. (of this report) Unclassified	20. SECURITY CLASSIF. (of this page) Unclassified	21. NO. OF PAGES 79	22. PRICE \$6.00

For sale by National Technical Information Service, Springfield, Virginia 22161